ACS Sustainable Chemistry & Engineering

pubs.acs.org/journal/ascecg

Research Article

Chitosan-Derived Nitrogen-Doped Carbon Electrocatalyst for a Sustainable Upgrade of Oxygen Reduction to Hydrogen Peroxide in UV-Assisted Electro-Fenton Water Treatment

Giorgia Daniel,[⊥] Yanyu Zhang,[⊥] Sonia Lanzalaco, Federico Brombin, Tomasz Kosmala, Gaetano Granozzi, Aimin Wang, Enric Brillas, Ignasi Sirés,* and Christian Durante*

Cite This: *ACS Sustainable Chem. Eng.* 2020, 8, 14425−14440

Read Online

ACCESS | Metrics & More | Article Recommendations | Supporting Information

ABSTRACT: The urgency to move from critical raw materials to highly available and renewable feedstock is currently driving the scientific and technical developments. Within this context, the abundance of natural resources like chitosan paves the way to synthesize biomass-derived nitrogen-doped carbons. This work describes the synthesis of chitosan-derived N-doped mesoporous carbon in the absence (MC-C) and presence (N-MC-C) of 1,10-phenanthroline, which acted as both a porogen agent and a second nitrogen source. The as-prepared MC-C and N-MC-C were thoroughly characterized and further employed as catalytic materials in gas-diffusion electrodes (GDEs), aiming to develop a sustainable alternative to conventional GDEs for H_2O_2 electrogeneration and photoelectro-Fenton (PEF) treatment of a drug pollutant. N-MC-C presented a higher content of key surface N-functionalities like the pyrrole group, as well as an increased graphitization degree and surface area (63 vs 6 m^2/g), comparable to commercial carbon black. These properties entailed a superior activity of N-MC-C for the oxygen reduction reaction, as confirmed from its voltammetric behavior at a rotating ring-disk electrode. The GDE prepared with the N-MC-C catalyst showed greater H_2O_2 accumulation, attaining values close to those obtained with a commercial GDE. N-MC-C- and MC-C-derived GDEs were employed to treat drug solutions at pH 3.0 by the PEF process, which outperformed electro-oxidation. The fastest drug removal was achieved using N-MC-C, requiring only 16 min at 30 mA/cm^2 instead of 20 min required with MC-C. The replacement of the dimensionally stable anode by a boron-doped diamond accelerated the degradation process, reaching an almost complete mineralization in 360 min. The main degradation products were identified, revealing the formation of six different aromatic intermediates, alongside five aliphatic compounds that comprised three nitrogenated structures. The initial N was preferentially converted into ammonium.

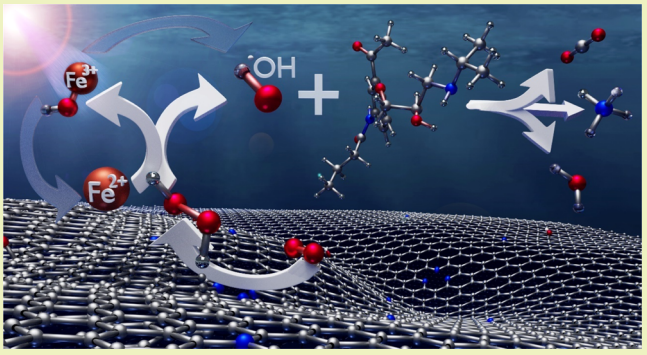

KEYWORDS: *biomass, electrochemical water treatment, gas-diffusion electrode, nitrogen-doped carbon, organic pollutant, oxygen reduction reaction*

INTRODUCTION

Lately, selected single atoms[1] as well as polyatomic Co-based compounds[2−4] have been successfully tested to electrocatalyze the two-electron oxygen reduction reaction (ORR, reaction 1) to hydrogen peroxide.[5]

$$O_{2(g)} + 2H^+ + 2e^- \leftrightarrows H_2O_2 \qquad E^0 = 0.695\ V \qquad (1)$$

Nonetheless, the development of metal-free electrocatalysts derived from cheap and environmentally friendly biomasses for ORR promotion has become a relevant topic,[6] especially within the context of circular economy. Carbon-based materials combine low cost and low environmental impact with high stability, features that make them suitable candidates for H_2O_2 generation in actual devices.[7−9] Likewise, porous carbonaceous materials with N-[10] or S-containing[11] surface functionalities, or both,[12−14] have shown promising electroactivity and selectivity for reaction 1.

To obtain nitrogenated carbon catalysts with high ORR performance and selectivity, three aspects need to be taken into account: (a) the type of N species, which determine the selectivity and the activity of the reaction sites;[10] (b) the architecture, in particular the surface area and porous structure; and (c) the degree of graphitization, which

Received: June 10, 2020
Revised: August 18, 2020
Published: August 25, 2020

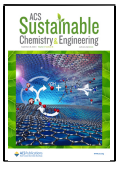

determines the conductivity and stability of the material. Both experimental studies and theoretical calculations confirmed that the ORR activity of nitrogen-doped carbon materials originates from the charge delocalization of the carbon atoms due to nitrogen incorporation, which facilitates oxygen adsorption and reduction. The activity was reported to be highly dependent on the doping level and types of nitrogen atoms.[10,12] Nitrogen functional groups can be pinned onto the carbon surface following three different strategies: (i) postfunctionalization of undoped carbon by means of ion implantation,[15] ball milling,[16] or grafting;[17] (ii) simultaneous carbonization and doping feasible via activation procedures like ammonia pyrolysis;[18] and (iii) use of a suitable carbon/nitrogen precursor to carry out the pyrolysis process.[12,13,19−22] Such precursors are N-containing organic molecules or polymers, such as 1,10-phenanthroline and polyaniline, but a plethora of examples starting from biomasses can be found in the literature.[5,23] Examples of transformation of N-containing biomass into N-doped carbons for ORR include the use of cellulose, algae, flowers, fruits, or bamboo.[24−32]

Considering any new carbonaceous electrocatalyst of interest, a simple cathode for massive H_2O_2 production could be prepared by coating a three-dimensional substrate, such as a carbon felt.[20,33] This type of substrate enhances the hydrodynamics and mass transport of oxygen,[34] which must be continuously dissolved in the aqueous solution by conventional[33,35,36] or advanced[37] means. Alternatively, the incorporation of an air chamber to the reactor enables a much greater oxygen concentration, thereby enhancing the H_2O_2 production.[5] In such a setup, either oxygen or air would be fed to a hydrophobized microporous[38] or macroporous[39] substrate coated with the electrocatalyst, the ensemble being called gas-diffusion electrode (GDE).

Hitherto, GDEs for H_2O_2 electrogeneration have been mostly manufactured using carbon black produced via hydrocarbon pyrolysis,[2,40−44] although other carbon materials like carbon nanotubes[3,4,45] or graphene[46] have also been employed. Fewer insights have been provided on mesoporous carbon,[12,13] whose ordered structure can minimize the residence of the generated H_2O_2 in the reaction zone.[47] Currently, the H_2O_2 production with GDEs finds its main application in water treatment, especially for the degradation of hardly biodegradable organic pollutants through advanced oxidation processes like electro-Fenton (EF) one.[48−50] In EF, the very reactive $^{\bullet}OH$ generated from Fenton's reaction 2 allows overcoming the limitations of conventional technologies.[51]

$$Fe^{2+} + H_2O_2 \rightarrow Fe^{3+} + {}^{\bullet}OH + OH^- \quad (2)$$

An upgraded version of EF involves the concomitant exposure of the treated solution to UVA light, causing the photoelectro-Fenton (PEF) process,[52] whose main contribution is the following photoinduced Fe^{2+} regeneration, favoring its immediate consumption via reaction 2[3,4,53,54]

$$[Fe(OH)]^{2+} + h\nu \rightarrow Fe^{2+} + {}^{\bullet}OH \quad (3)$$

N-doping of carbons to manufacture GDEs suitable for EF or PEF has been scarcely studied. The presence of N increased the electroactivity of a cathode composed of carbon nanotubes coated with graphene, ending in a faster degradation of dimethyl phthalate by EF.[55] N-doped carbon prepared from 1*H*-1,2,4-triazole-3,5-diamine showed the highest ORR rate among other materials, yielding a faster EF degradation of sulfathiazole.[56] The number of studies is even lower in the case of biomass-derived carbons for H_2O_2 production with GDEs. As far as we know, Liao et al.[57] have reported the only article on the topic, which discusses the performance of a GDE made of N-doped mesoporous carbon coming from bean dregs. They simply used the cathode to generate H_2O_2 for formaldehyde degradation, which means that the investigation of biomass-derived GDEs in EF and PEF is a quite unexplored field.

Aiming to conceive more eco-friendly EF and PEF approaches for water treatment, herein, chitosan has been chosen as a suitable N-containing biopolymeric gel precursor for preparing a mesoporous carbon material (MC-C) in virtue of its biocompatibility, biodegradability, and high N content (7.1%). It is worth noticing that raw chitosan has been included in some EF systems so far, mainly in the form of a composite with iron species to promote heterogeneous Fenton's reaction,[58] although as far as we know it was never incorporated in the form of carbon powder. Chitin and its derivative chitosan are among the most abundant organic compounds in nature that are easily obtained from crustacean shells and purified further,[59] which make them adequate for a wide range of applications.[60] The physicochemical characterization of the synthesized catalysts was performed by different techniques. Their ability to electrogenerate H_2O_2 was assessed by means of cyclic voltammetry (CV) and linear sweep voltammetry (LSV), as well as via bulk electrolysis. In addition, the comparative degradation ability of the two catalysts was investigated by treating 150 mL of acebutolol solutions at acidic pH. The selection of the contaminant is justified by the growing complexity of global water pollution associated with pharmaceuticals due to both the diversity of target molecules and large volume of effluents. Standard water treatments are frequently unable to ensure total detoxification, which urges for more advanced technologies.[61] The hypotensive and antiarrhythmic acebutolol is excreted mostly in its unmetabolized form, hence it is accumulated alongside its intermediates in surface water,[62] as well as in sewage treatment plant effluents, evidencing a low biodegradability.[63] This represents a serious threat because acebutolol is toxic to aquatic organisms[64] and causes lupus-like syndrome.[65] Herein, the PEF process was assessed for the first time for acebutolol remediation.

MATERIALS AND METHODS

Chemicals. Chitosan (>98%, Life Science Aldrich) and 1,10-phenanthroline (>99.5%, TCI) were used as received. Other reagents employed for the synthesis of catalysts were pure ethanol (>99.8%, Fluka), Nafion (5 wt % in a mixture of lower aliphatic alcohols and water, Sigma-Aldrich), acetic acid (>99.8%, Sigma-Aldrich), acetone (>99.5%, Sigma-Aldrich), H_2SO_4 (95%, Fluka), and NaOH (>99%, VWR). Each catalyst was mixed with ethanol (96%, Panreac) and polytetrafluoroethylene (PTFE, 60 wt % solution, Sigma-Aldrich), following the procedure described below, to manufacture a GDE. The specific reagents required for the bulk electrolytic trials were acebutolol (*N*-[3-acetyl-4-[2-hydroxy-3-(propan-2-ylamino)propoxy]-phenyl]butanamide) in the form of a hydrochloride salt ($C_{18}H_{28}N_2O_4$·HCl, CAS number: 34381-68-5, Sigma-Aldrich), Na_2SO_4 (anhydrous, Merck), and $FeSO_4·7H_2O$ (Panreac). Acetonitrile and KH_2PO_4 used to quantify acebutolol, as well as CH_2Cl_2 employed in gas chromatography−mass spectrometry (GC/MS), were of high-performance liquid chromatography (HPLC) grade from Panreac. Other chemicals needed for the analytical procedures described below included Ti(IV) oxysulfate (technical grade, Sigma-Aldrich) to determine the H_2O_2 concentration and phenol (99.5%, Sigma-Aldrich), sodium nitroprusside dehydrate (Merck), and

https://dx.doi.org/10.1021/acssuschemeng.0c04294
ACS Sustainable Chem. Eng. 2020, 8, 14425−14440

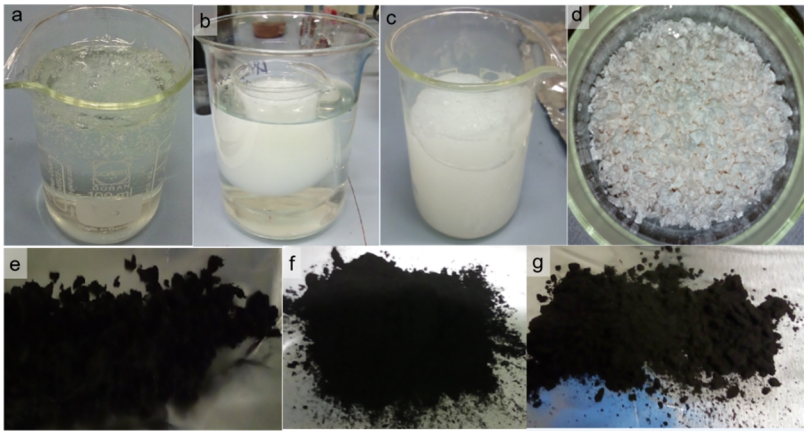

Figure 1. Different stages during the synthesis of MC-C catalysts: (a) chitosan viscous solution, (b) hydrogel coagulation, (c) chitosan hydrogel, (d) hydrogel after freeze-drying, (e) dried hydrogel after pyrolysis at 400 °C, (f) first pyrolysis product after milling, and (g) product after pyrolysis at 900 °C.

ethylenediaminetetraacetic acid disodium salt dihydrate (99%, Alfa Aesar) to quantify the ammonium ion. Ultrapure water for the synthesis, manufacture, electrolysis, and analysis was obtained from a Millipore Milli-Q system (Merck).

Synthesis of Catalysts. The synthesis of carbon electrocatalysts from chitosan was accomplished by modifying the procedure reported in the literature.[66,67] Chitosan was employed as a source of both carbon and nitrogen as it is composed of repeating units of randomly distributed β-(1 → 4)-linked D-glucosamine and *N*-acetyl-D-glucosamine. The synthesis consisted of the formation of a chitosan hydrogel followed by the removal of the solvent by freeze-drying and pyrolysis of the resulting material. The hydrogel synthesis involved the dispersion of the chitosan powder (1.8 g) in an acetic acid solution (100 mL, 2 vol %), and the resulting mixture was vigorously stirred to ensure complete solubilization. In fact, at acidic pH, the amine groups in the *N*-acetyl-β-(D)-glucosamine moiety are protonated to ammonium (pK_a ($-NH_3^+$) = 6.3),[68] which disrupts the hydrogen bonds between the polymer chains and leads to the collapse of the chitosan crystalline structure and to the solubilization of the polymer in water, finally obtaining a transparent, homogeneous, and viscous solution (Figure 1a). The hydrogel formation then occurred by slowly pouring a 1 M NaOH solution into the chitosan viscous solution. As the diffusion of OH^- ions is slow, the gelation was not instantaneous, but the gelation front advanced at the hydrogel/NaOH solution interphase as the hydroxide ions diffused through the chitosan solution (Figure 1b). The alkaline pH favored the deprotonation of the $-NH_3^+$ groups, promoting the interaction between polymeric chains by hydrogen interactions along with the incorporation of the solution between the chitosan chains, yielding the hydrogel. Once the gelation was concluded, the hydrogel was repetitively rinsed with water until a neutral pH was reached (Figure 1c). Subsequently, the gel was cut into small pieces with a chisel and freeze-dried to remove all water. The dried gel (Figure 1d) was then thermally treated in a two-step pyrolysis procedure.[28] The gel was heated in a Carbolite tubular furnace with a 75 sccm (standard cm^3/min) N_2 flux at 100 °C for 1 h, after which the temperature was raised up to 400 °C at a rate of 5 °C/min and kept at that temperature for 2 h. The resulting powder (0.72 g) (Figure 1e) was ground by vibromilling (Retsch MM 400, four steps of 4 min/10−25 Hz) (Figure 1f) and eventually repyrolyzed at 900 °C for 2 h under a nitrogen atmosphere (Figure 1g). The obtained carbon powder (MC-C, 0.52 g) was washed with water and ethanol, dried at 80 °C overnight, and ground by vibromilling.

Alternatively, phenanthroline was used as a secondary source of nitrogen, which was added (0.3 g) to the initial chitosan/acetic acid solution and the mixture was stirred and allowed to gel after the addition of NaOH solution. This procedure allowed fine dispersion of phenanthroline all over the hydrogel, avoiding the preferential functionalization of the resulting carbon catalyst and formation of a heterogeneous material. It is worth noting that part of the added phenanthroline was washed away during the neutralization procedure with deionized water, as was confirmed by the presence of the typical UV−vis adsorption pattern of phenanthroline in the washing water (Figure S1). Conversely, phenanthroline was detected only in traces in the water extracted during the freeze-drying procedure (Figure S1). The resulting dried gel was subjected to double pyrolysis at 400 and 900 °C, followed by ball milling as in the previous case. The catalyst obtained starting from 1,10-phenanthroline and chitosan will be denoted from now on as N-MC-C.

Physicochemical Characterization of Catalyst Powders. Brunauer−Emmett−Teller (BET) analysis, isotherm, and pore distribution were performed via nitrogen adsorption−desorption at 77 K using the Micromeritics ASAP2020. The surface area was determined from the desorption curve in a multipoint BET analysis, whereas the pore distribution was analyzed with a slit/cylindric pore NLDFT equilibrium model. Elemental analysis (EA) was carried out using a Thermo Scientific Flash 2000 device. Transmission electron microscopy (TEM) images were obtained using a FEI Tecnai G2 transmission electron microscope operating at 100 kV. X-ray photoemission spectroscopy (XPS) measurements were performed in an UHV chamber (base pressure < 5×10^{-10} mbar), equipped with a double anode X-ray source (Omicron DAR-400), a hemispherical electron analyzer (Omicron EIS-125) at room temperature, using nonmonochromatized Mg Kα radiation ($h\nu$ = 1253.6 eV), and a pass energy of 50 and 20 eV for the survey and single spectral windows, respectively. To perform the XPS measurements, 2.5 mg of carbon powders were dispersed in 1 mL of ethanol and then sonicated for 10 min in order to obtain good dispersions; the solutions were then drop-casted onto polycrystalline copper (with a diameter of 6 mm). Raman scattering experiments were conducted with a DXR Raman microscope system (Thermo Fisher Scientific), with a 532 nm laser as the photoexcitation source. The size of the laser spot on the sample was about 25 μm and the power at the sample was 0.1, 0.5, or 1.0 mW.

Electrochemical Characterization of Catalyst Powders. CV and LSV analyses at a rotating ring disk electrode (RRDE, Metrohm, and a 5 mm diameter glassy carbon (GC) disk + Pt ring, with a collection efficiency of 25%) were performed in both Ar-purged and O_2-saturated 0.0005 M H_2SO_4 + 0.050 M Na_2SO_4 solutions using an Autolab model 101 N potentiostat/galvanostat. A three-electrode configuration was used, consisting of a GC disk (geometric area: 0.196 cm^2) as a working electrode, a graphite rod as a counter electrode, and a reversible hydrogen electrode (RHE) as a reference electrode. The latter was freshly prepared before each experiment and consisted of a Pt wire mesh sealed to the closed end of a capillary glass tube and refilled with the electrolyte solution from the other open end. H_2 was directly electrogenerated at the Pt wire mesh so that half

https://dx.doi.org/10.1021/acssuschemeng.0c04294
ACS Sustainable Chem. Eng. 2020, 8, 14425−14440

of the Pt mesh was exposed to the H_2 bubble confined between the electrolyte solution and the closed end of the capillary.[69]

The MC-C and N-MC-C catalysts were characterized as thin films prepared by drop-casting an ink (20 μL) of the corresponding carbon powder on a GC disk. Before the drop casting, the GC was polished to a mirror finish with Struers silicon carbide papers of decreasing grain size (grit: 500, 1000, 2400, and 4000), followed by diamond paste (3, 1, and 0.25 mm particle size), and repeatedly washed and sonicated (10 min each time) in ethanol for removing all contaminants.

All the electrochemical assays were carried out with an optimized loading of 0.6 mg/cm^2. The electrolyte was purged with Ar before each measurement, whereas for the ORR test, high-purity O_2 gas was bubbled through the electrolyte for at least 1 h to ensure O_2 saturation. The number of electrons transferred during ORR was determined by the RRDE technique. Before data acquisition, the electrocatalysts were first activated by cycling the electrode in the solvent potential window at 200 mV/s until obtaining a stable cyclic voltammogram.

Fabrication of Gas-Diffusion Cathodes. A GDE was prepared from each type of synthesized powder using the spraying method.[3,4] An appropriate amount (0.1 g) of MC-C or N-MC-C powder was ultrasonically dispersed with PTFE and ethanol for 45 min to obtain an ink (~20 mL). Carbon cloth (~8 cm^2 geometric area, BASF B1ASWP), degreased in ethanol and then dried at 60 °C for 3 min, was used as a substrate to spray the ink. An air-brush gun fed with N_2 gas was employed to apply several layers, until the ink was finished. After each layer, the material was dried at 60 °C for 3 min and then weighed. The sample was pressed at 2 ton for 45 s, annealed at 400 °C for 60 min under a nitrogen atmosphere, and finally cooled down under ambient conditions. The overall weight increment in each GDE was ~80 mg (i.e., MC-PTFE loading is 9.7 mg/cm^2). In order to use any new GDE, it was first activated by conducting a galvanostatic polarization in 0.050 M Na_2SO_4 at pH 3.0 for 60 min.

The morphological characteristics of the GDEs before and after use were assessed by scanning electron microscopy (SEM) using a JEOL JSM-7100F field-emission microscope equipped with an energy-dispersive X-ray spectroscopy analyzer. All images were obtained at a voltage of 20.0 kV.

Bulk Electrolyses and Analyses. Electrolytic trials were conducted for several hours in the absence and presence of pollutants to evaluate the H_2O_2 electrogeneration ability of GDEs and the degradation performance of different processes, respectively. In all these trials, a given GDE (3 cm^2) prepared as described above was placed in a tubular polypropylene housing that received compressed air pumped at 36 L/h, and such cathode was connected to the anode (3 cm^2). The latter consisted of a RuO_2-based plate (i.e., dimensionally stable electrode, DSA) from NMT Electrodes in most of the trials, although boron-doped diamond (BDD) from NeoCoat was also employed in some cases. The distance between the anode and cathode was 1.0 cm. The assays were performed in an undivided glass cell, which was placed onto a magnetic stirrer operated at 700 rpm and contained 150 mL of solution at pH 3.0 and thermostated at 25 °C. All treatments were made in the presence of 0.050 M Na_2SO_4 as a background electrolyte and, when required, acebutolol was added at a concentration of 0.046 mM, that is, 10 mg/L total organic carbon (TOC). In EF and PEF, the Fe^{2+} catalyst was added before starting the electrolysis at a concentration of 0.50 mM. In the photoassisted treatment, the solution was illuminated with UVA photons from a 6 W Philips tubular lamp (λ_{max} = 360 nm, irradiance = 5 W/m^2) placed above the reactor near the liquid surface. Constant current was always supplied by an Amel 2051 potentiostat–galvanostat, whereas the cell voltage (E_{cell}) was continuously displayed by a Demetres 605 multimeter.

When required, the pH of solutions was measured with a Crison GLP 22 pH-meter. Colorimetric analysis of the complex formed between Ti(IV) and H_2O_2 was done using an Unicam UV/vis spectrophotometer set to λ_{max} = 408 nm, with solutions thermostated at 25 °C. The content of ammonium ion was measured with the same equipment, according to the indophenol blue method, at λ_{max} = 630 nm.[3] TOC was determined using the nonpurgeable organic carbon (NPOC) mode of a Shimadzu TOC-VCNS analyzer. Acebutolol concentration was determined by reversed-phase HPLC, with a Waters 600 apparatus equipped with a C18 column at 35 °C connected to a photodiode array detector. A well-resolved peak appeared at a retention time of 4.6 min (λ = 235 nm). The mobile phase was a mixture of acetonitrile (40 vol %) and water (10 mM KH_2PO_4 at pH 3.0, 60 vol %), circulating at 1.0 mL/min. Trials were made in duplicate and injections in triplicate to correctly assess the drug disappearance. Hence, average values are shown in the figures alongside the error bars (95% confidence level). The final carboxylic acids were quantified as previously reported, by injecting the samples into the same chromatograph system but equipped with an Aminex column.[39] Before each analysis, the samples were conditioned by filtration with PTFE filters (13 mm × 0.45 μm, Whatman).

Current efficiency (CE) values during H_2O_2 electrogeneration were calculated from the applied charge, according to eq 4[5]

$$\mathrm{CE\ (in\ \%)} = \frac{2F[\mathrm{H_2O_2}]V}{1000M(\mathrm{H_2O_2})Q}100 \tag{4}$$

where 2 is the stoichiometric number of electrons transferred for ORR to form H_2O_2, F is the Faraday's constant (96,487 C/mol), $[H_2O_2]$ is the concentration of accumulated H_2O_2 (mg/L), V is the volume of the treated solution (L), 1000 is a conversion factor, $M(H_2O_2)$ is the molecular weight of H_2O_2 (34 g/mol), and Q is the charge consumed during electrolysis.

The mineralization CE (MCE) for each trial at a given electrolysis time t (in h) and applied current I (in A) was calculated as follows[70]:

$$\mathrm{MCE\ (in\ \%)} = \frac{nFV(\Delta\mathrm{TOC})_{exp}}{4.32 \times 10^7 mIt}100 \tag{5}$$

where n accounts for the number of electrons consumed for the overall mineralization of the drug, $\Delta(TOC)_{exp}$ is the observed TOC decay (in mg/L), 4.32×10^7 is a conversion factor (= 3600 s/h × 12,000 mg C/mol), and m is the number of carbon atoms of acebutolol (18 atoms).

The specific energy consumption per unit TOC mass (EC_{TOC}) was obtained as follows[70]:

$$\mathrm{EC_{TOC}\ (in\ kW\ h/g\ TOC)} = \frac{E_{cell}It}{V(\Delta\mathrm{TOC})_{exp}} \tag{6}$$

where E_{cell} is the average cell voltage (in V).

The primary reaction products were identified by GC/MS. For this, samples collected after selected electrolyses were prepared by liquid–liquid extraction with CH_2Cl_2 as an organic solvent.[36] GC/MS analysis was made in the electron impact mode at 70 eV with an Agilent Technologies system: a 6890N gas chromatograph with a 7683B series injector was connected to a 5975 mass spectrometer. Nonpolar Teknokroma Sapiens-X5.ms and polar HP-INNOWax columns, both with dimensions of 0.25 μm and 30 m × 0.25 mm (i.d.), were used. When using the former, the conditions were as follows: temperature ramp starting at 36 °C for 1 min and increasing up to 320 °C at 5 °C/min (holding time: 10 min); the temperature of the inlet, source, and transfer line was 250, 230, and 300 °C, respectively, and the analyses were made by a splitless (0.7 min) injection, with a run time of 67.80 min. When the latter was employed, the conditions were analogous, but the final temperature was 250 °C, with 250 °C as the temperature of the transfer line and 93.80 min as the run time.

RESULTS AND DISCUSSION

Characterization of Synthesized Catalysts. Nitrogen-doped carbon is a term commonly accepted by the scientific community to classify carbon powder containing nitrogen functional groups. In the present paper, pyrolysis of the pure dried chitosan hydrogel as well as of the dried hydrogel impregnated with 1,10-phenanthroline yielded two samples,

https://dx.doi.org/10.1021/acssuschemeng.0c04294
ACS Sustainable Chem. Eng. 2020, 8, 14425−14440

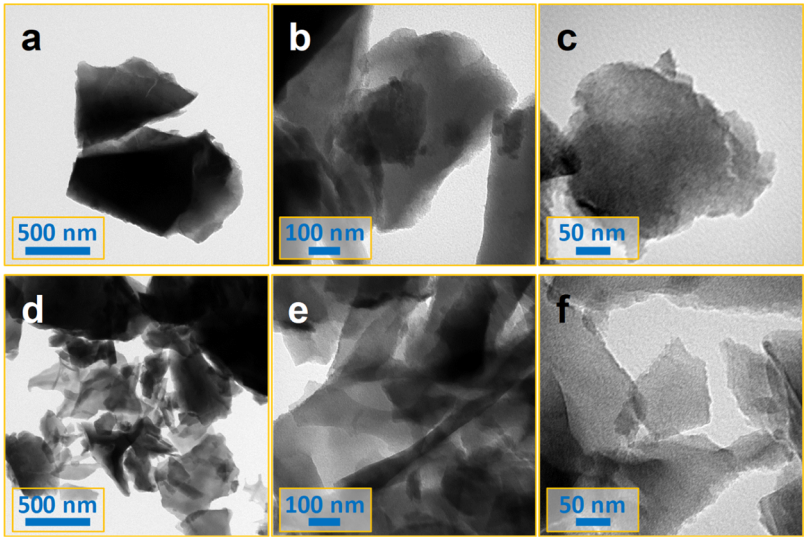

Figure 2. TEM images of (a–c) MC-C and (d–f) N-MC-C catalysts.

Table 1. Chemical and Textural Properties of Activated Carbons

sample	C[a] (%)	H[a] (%)	N[a] (%)	A_{BET}[b] (m^2/g)	V_{TOT}[b] (cm^3/g)	V_{μ}[b] (cm^3/g)	V_{meso}[b] (cm^3/g)	V_{DFT}[b] (cm^3/g)
MC-C	76.44	0.81	6.81	6	0.013	0.002	0.005	0.007
N-MC-C	79.39	1.73	4.62	63	0.065	0.021	0.017	0.038

sample	C 1s[c] (at %)	O 1s[c] (at %)	N 1s[c] (at %)	N_{imine}[c] (%)	$N_{pyridinic}$[c] (%)	N_{aminic}[c] (%)	$N_{pyrrolic}$[c] (%)	$N_{graphitic}$[c] (%)	N–O[c] (%)
MC-C	78.5	19.1	2.4	29.3	19.5	22.7	22.0	3.5	3.0
N-MC-C	81.6	15.3	3.1	23.1	9.2	19.0	30.7	12	6.1

[a]EA determined by the CHN analyzer. [b]Textural properties determined from nitrogen adsorption–desorption isotherms. [c]EA expressed in atomic percentage and nitrogen functionalities determined from XPS analysis and N 1s spectral deconvolution.

denoted MC-C and N-MC-C, respectively. The three-dimensionality of chitosan hydrogels allows the fine dispersion of additives inside the gel structure, which can improve the functionalization of the carbon structure and enhance the textural properties resulting from thermal treatment. A double-step pyrolysis, at 400 and 900 °C, was employed for decreasing the burn off of the material, and the resulting black powder was characterized after ball milling.

Figure 2 highlights the TEM images of the two types of carbon powder at different magnifications. The structure of the MC-C sample is characterized by the overlay of compact carbon lamellae (Figure 2a–c), in which any pore structure is clearly visible. The morphological features of MC-C are in part superimposable with those of N-MC-C (Figure 2d–f). However, the lamellar structures in the latter case are characterized by a less packed and compact structure, presenting more jagged edges.

Table 1 reports the elemental analyses of the synthetized carbons. MC-C, prepared by employing solely chitosan both as a carbon and nitrogen precursor, shows a nitrogen fixation of almost 7%, as evidenced by the CHN analysis. Then, it must be clear that the notation MC-C simply means that an additional N-rich precursor was not employed during the synthesis. Also, the oxygen content, which in the first approximation can be calculated as the residual mass percentage, is sensitively high (~16%). Therefore, it is reasonable to infer that the MC-C carbon was rich in nitrogen and oxygen functional groups, which are extremely important as active sites to electrocatalyze some reactions as well as for increasing the wettability of the electrode material during the electrocatalytic tests. A close comparison with the values obtained for the N-MC-C sample (Table 1) allows noticing that, when 1,10-phenanthroline was used as a secondary nitrogen source during the chitosan hydrogel preparation, the resulting material had a higher carbon and hydrogen content but a lower nitrogen (<5%) and oxygen (<15%) percentage as compared to MC-C. We can presume that the pyrolysis of 1,10-phenanthroline generates small gaseous molecules such as NO, NO_2, and CO, which may act as oxidizing agents with the ability to react with the amorphous part of the carbon structure, that is, the sp^3 carbon atoms bonded to nitrogen and oxygen functional groups, while the more graphitic sp^2 carbon atoms are preserved, being less prone to react with in situ-generated reactive species.

The nitrogen adsorption/desorption isotherms at 77 K for MC-C belong to type II, which is characteristic of nonporous or macroporous materials having a relatively small external surface (Figure 3a). However, the TEM pictures do not show the presence of macropores (Figure 2a–c), which would correspond to pores with diameters wider than 50 nm, being reasonable to conclude that MC-C can be classified as a nonporous carbon material. The sample showed a non-reversible desorption behavior with an open hysteresis loop classified as type-H4, which is often attributed to narrow slit-like pores.[71] The very low value of mesopore volume (Table 1) can be associated with the collapse of the mesopore structure during the gas desorption or to the entrapment of N_2 gas in narrow pores formed between two carbon foils, which could also explain the open hysteresis.[72] However, the experiment was repeated a second time, showing the very same behavior and hence the first hypothesis of a carbon structure collapse can be disregarded, the irreversible confinement of N_2

https://dx.doi.org/10.1021/acssuschemeng.0c04294
ACS Sustainable Chem. Eng. 2020, 8, 14425–14440

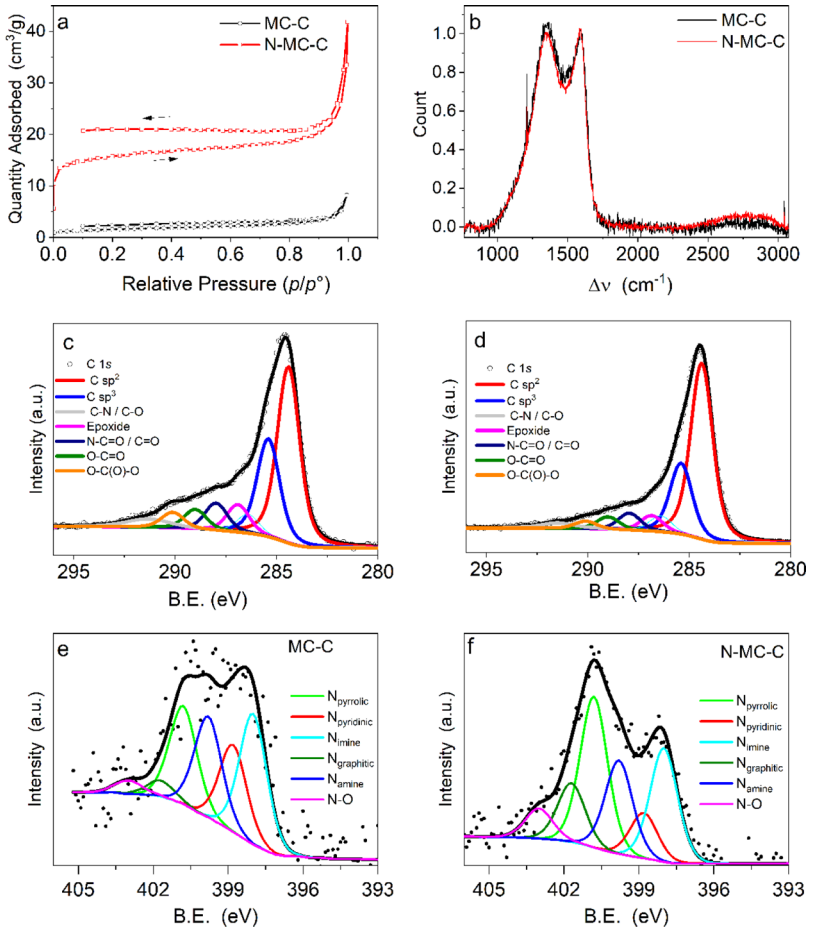

Figure 3. (a) Nitrogen adsorption/desorption isotherms of MC-C and N-MC-C catalysts; (b) Raman spectra for both materials; C 1s XPS core-level spectra for (c) MC-C and (d) N-MC-C catalysts; N 1s XPS core-level spectra for (e) MC-C and (f) N-MC-C. In (c–f), deconvolution signals are also shown.

molecules between carbon foils being the most probable explanation. The extrapolated BET surface area was as small as A_{BET} = 6 m^2/g. Figure 3a also reports the type II nitrogen adsorption/desorption isotherm for N-MC-C. Similarly, in this case, the open hysteresis loop can be classified as type-H4, and an analogous conclusion can be drawn regarding the open hysteresis. It is worth noting that the presence of 1,10-phenanthroline in the dried hydrogel affected very positively the BET surface area, which was enhanced up to 63 m^2/g in N-MC-C. In this case, the more pronounced uptake at low $p/p°$ can be associated with an enhanced adsorbent–adsorbate interaction in narrow micropores.[72] The large area was directly related to the increased porosity (Table 1), which was mainly due to micropores (d < 2 nm, V_μ = 0.021 cm^3/g), along with a mesopore fraction (2 nm < d < 50 nm, V_{meso} = 0.017 cm^3/g). The formation of micropores and mesopores or the simple opening of clogged pores can be associated with the reaction of NO, NO_2, and CO gaseous species, generated during the pyrolysis of 1,10-phenanthroline with the carbon structure while CO_2 is released.[73,74] The pronounced uptake at high $p/p°$ is indicative of the presence of macropores (d > 50 nm), which cannot be in any case evaluated in terms of pore volume and area by the adopted model. However, the presence of a more open and accessible structure finds a confirmation in the TEM images described above. Note that the higher porosity of N-MC-C as compared to MC-C is also evident from the greater total volume (V_{TOT}) summarized in Table 1 (0.065 vs 0.013 cm^3/g, respectively). Therefore, while MC-C is a nonporous carbon material, N-MC-C can be classified as a carbon material with low porosity and textural properties similar to those of commercial carbon black (A_{BET} = 67 m^2/g, V_μ = 0.015 cm^3/g, and V_{meso} = 0.137 cm^3/g).

The MC-C and N-MC-C samples were characterized by Raman spectroscopy, which allows elucidating the possible differences in the order and aggregation degree of sites with sp^2 hybridization and, more in general, informs about the amorphous and graphitized degree of a carbon material (Figure 3b).[75] Soft and hard carbon materials typically show two main bands: the D1 (disorder) band at ~1350 cm^{-1} and the G (graphitic) band at ~1595 cm^{-1}, as also corroborated for the MC-C and N-MC-C samples. The 2D peak at ~2680 cm^{-1}, ascribed to an out-of-plane vibration mode and generally present in graphite, single-layer graphene, or highly graphitized carbon, is missing, but a broad band between 2400 and 3000 cm^{-1} is present in both samples. The spectral deconvolution revealed the existence of four bands after baseline subtraction and normalization to the maximum of the G band. The two further bands D4 and D3 account for polyenes or ionic impurities and amorphous carbon, respectively. The resulting I_{D1}/I_G band intensity ratio was close to one for both samples (Figure S2). According to the Tuinstra–Koenig model, the following relationship is satisfied[76]:

https://dx.doi.org/10.1021/acssuschemeng.0c04294
ACS Sustainable Chem. Eng. 2020, 8, 14425–14440

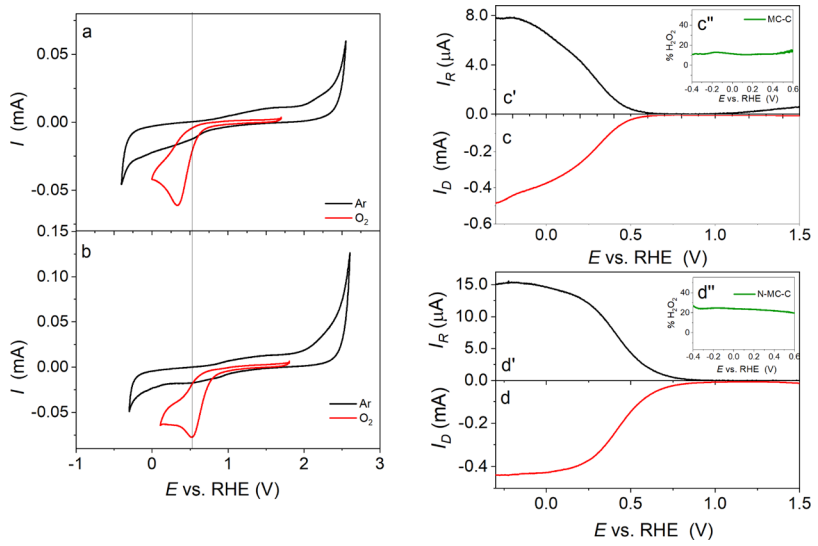

Figure 4. Electrochemical data for the investigated materials, drop-cast on GC (catalyst loading: 0.3 mg/cm^2), in an Ar-purged and O_2-saturated 0.0005 M H_2SO_4 + 0.050 M Na_2SO_4 electrolyte. Cyclic voltammograms of (a) MC-C and (b) N-MC-C, at ν_{scan} = 20 mV/s. Linear sweep voltammograms at RRDE, with ν_{scan} = 10 mV/s and ω = 1600 rpm, of (c) MC-C and (d) N-MC-C. (c′,d′) Ring current, at E_{ring} = 1.50 V vs RHE, and (c″,d″) H_2O_2 selectivity during LSV in an O_2-saturated electrolyte, of (c′,c″) MC-C and (d′,d″) N-MC-C.

$$\frac{I(\mathrm{D1})}{I(\mathrm{G})} = \frac{C(\lambda)}{L_a} \tag{7}$$

where $C(\lambda) = -12.6 + (0.033\lambda) \approx 50$ Å, (λ = 532 nm), and thus the band intensity ratio can be used to determine the size of the graphite nanocrystallites, which was 4.7 and 5.0 nm for MC-C and N-MC-C, respectively. A close comparison of the two spectra allows observing two main differences: (i) the D1 intensity was higher in the MC-C spectrum than in the N-MC-C one and (ii) the valley (minimum intensity point) between the D1 and G bands was higher in MC-C than in N-MC-C. Both characteristics lead to the conclusion that N-MC-C was more graphitized than MC-C. This can be further confirmed by considering the D3 band area, responsible for the amorphous carbon, which is lower in N-MC-C (37.6 normalized counts) with respect to MC-C (41.6 normalized counts).

XPS analysis confirmed the presence of nitrogen, oxygen, and carbon in both samples (Table 1 and Figure S3). The higher percentage of oxygen in MC-C with respect to N-MN-C confirmed that the introduction of 1,10-phenanthroline contributed to a greater graphitization. Figure 3c,d and Table S1 show the C 1s XPS data of the analyzed samples. The main carbon component at binding energy (B.E.) = 284.4 eV is attributed to C sp^2.[12,15,77] At a higher B.E. (285.4 eV), the peak corresponded to the sp^3 C−C bond. The higher sp^2/sp^3 ratio in N-MC-C as compared to the MC-C sample is in agreement with the observations from Raman analysis (Table S1). There was also a substantial amount of carbon bound to nitrogen and/or to oxygen (peak at 286.4 eV). Peaks at B.E. higher than 286.4 eV were due to carbon species bound to oxygen (C═O, O−C═O, and O−C(O)−O) or to both oxygen and nitrogen (C−N═O and N−C═O). the peak at 291.1 eV was due to the shakeup satellite (π−π*).

The N 1s spectra and their deconvolution in single peaks are reported in Figure 3e,f. EA determined from XPS data indicates a weight percentage of surface nitrogen of 2.6 and 3.4% for MC-C and N-MC-C, respectively, in contrast to the abovementioned CHN analysis, which is a bulk sensitive technique that detected a greater nitrogen content in the MC-C sample (Table 1). Therefore, it is reasonable to assert that in the MC-C catalyst, the nitrogenated functional groups are mostly confined in the bulk of the carbon material, whereas pyrolysis of the chitosan hydrogel carried out in the presence of 1,10-phenanthroline leads to a higher surface nitrogen content, thereby providing a higher number of available active sites. This is a key finding that justifies the presence of the additional N-containing precursor during the synthesis as the resulting surface N-functionalities are expected to induce a higher H_2O_2 electrogeneration. The speciation of the singular N 1s components evidences the presence of pyridinic, imine, amine, and pyrrolic nitrogen (Table 1). Graphitic and nitrogen oxide components were also present in lower percentages.[12,28] It is interesting to observe that the pyrrolic component significantly increases in N-MC-C. Both pyridinic and pyrrolic nitrogen are beneficial groups as they increase the carbon activity versus ORR and, more in particular, it is reported that pyrrolic nitrogen favors the bielectronic reduction of oxygen to hydrogen peroxide.[17,27,30]

Electroactivity of Chitosan-Derived Catalysts. MC-C and N-MC-C were both electrochemically characterized in 0.0005 M H_2SO_4 + 0.050 M Na_2SO_4 as a background electrolyte, aiming to determine their activity regarding the oxygen reduction and their corresponding selectivity toward H_2O_2 generation. Figure 4a,b compares the electrochemical behavior in Ar-purged and O_2-saturated electrolyte using MC-C and N-MC-C electrocatalysts, respectively. No redox signal appeared in the purged medium, whereas both materials showed electroactivity versus ORR, as deduced from the well-defined reduction peak that was visible in the presence of dissolved O_2. The O_2 reduction peak potential using N-MC-C (0.525 V vs RHE) was 190 mV more positive than that obtained with MC-C (0.335 V vs RHE). The smaller overpotential required for using N-MC-C informs about its higher activity with respect to MC-C, which can be attributed to the aforementioned greater content of nitrogen groups on the N-MC-C surface (Table 1).

https://dx.doi.org/10.1021/acssuschemeng.0c04294
ACS Sustainable Chem. Eng. 2020, 8, 14425−14440

The ORR may proceed through two pathways: one is a direct four-electron route, which consists of direct O_2 reduction to water without involvement of H_2O_2 (reaction 8), and the other is a two-step two-electron route in which H_2O_2 is first formed as an intermediate via the two-electron reaction 1, and then it can potentially undergo further reduction via reaction 9.[5]

$$O_{2(g)} + 4H^+ + 4e^- \leftrightarrows 2H_2O \qquad E^0 = 1.229\ V \tag{8}$$

$$H_2O_2 + 2H^+ + 2e^- \leftrightarrows 2H_2O \qquad E^0 = 1.763\ V \tag{9}$$

The selectivity toward the formation of H_2O_2 was evaluated by LSV using an RRDE in an O_2-saturated electrolyte at a scan rate of 10 mV/s and a rotation speed (ω) of 1600 rpm. During RRDE experiments, the potential of the disk electrode was swept to cathodic values, so the appearance of current (I_D) in the linear voltammogram using MC-C and N-MC-C confirmed the reduction of O_2, as this was the sole reducible species present in solution (Figure 4c,d, respectively). Because of the electrode rotation, the current increased until a limiting value (I_{lim}) was attained, which depended primarily on the electrode ω, the dissolved O_2 concentration (C_{O_2}), the O_2 diffusion coefficient (D_{O_2}), the solvent kinematic viscosity (ν), and the number of transferred electrons (n), according to the Koutecky–Levich equation[12]:

$$\frac{1}{I} = \frac{1}{I_k} + \frac{1}{I_{lim}} = \frac{1}{nFAkC_{O_2}} + \frac{1}{0.62nFA(D_{O_2})^{2/3}\nu^{-1/6}C_{O_2}\omega^{1/2}} \tag{10}$$

where I_k is the kinetic current and I_{lim} is the diffusion-limiting current. In such setup, the electrode rotation pushes the electrogenerated species toward the ring electrode, which is polarized at a fixed potential (E_{ring} = 1.50 V vs RHE), at which H_2O_2 can be easily reoxidized to H_2O. If H_2O_2 is generated at the disk electrode, it can be then detected at the ring electrode and a ring current (I_R) can be recorded in the cases of MC-C and N-MC-C (Figure 4c′,d′, respectively). The number of exchanged electrons can in principle be determined by plotting the reciprocal of the total instant current (I^{-1}) versus $\omega^{-1/2}$, whenever all the other specific parameters are known. However, this procedure can lead to misleading results when, for example, the catalyst layer is not homogeneous and sufficiently thin. Alternatively, the number of electrons involved in the ORR and the yield of hydrogen peroxide ($y_{H_2O_2}$) can be obtained from the I_D (in A) and I_R (in A) values measured at the RRDE, according to eqs 11 and 12[72]:

$$n = \frac{4I_D}{I_D + I_R/N} \tag{11}$$

$$y_{H_2O_2} = 100\frac{2I_R}{NI_D + I_R} \tag{12}$$

where N is the collection efficiency (N = 0.25). The half-wave potential, which can be determined from the RRDE measurements, confirmed the higher catalytic activity of N-MC-C ($E_{1/2}$ = 0.437 V) as compared to MC-C ($E_{1/2}$ = 0.288 V). Furthermore, the n values were 3.55 and 3.76, using N-MC-C and MC-C, respectively, which informs about the superior selectivity versus H_2O_2 generation using the former electrode. In fact, the hydrogen peroxide yields ($y_{H_2O_2}$, Figure 4c″,d″) were 25% (N-MC-C) and 11% (MC-C). At first sight, these values could seem to be far from n = 2, and $y_{H_2O_2}$ = 100% is ideally expected from an electrocatalyst that fully promotes the two-electron ORR, without further H_2O_2 reduction or simultaneous reaction 5. Nonetheless, the main goal within the context of this work was not the development of an optimum electrocatalyst for H_2O_2 electrosynthesis but the synthesis of a potentially cheaper and more eco-friendly material to electrogenerate sufficient amounts of H_2O_2 for its direct application in Fenton-based electrochemical water treatments. Therefore, bulk electrolyses were conducted in order to assess the ability of GDEs, prepared with the synthesized MC-C and N-MC-C, to accumulate H_2O_2.

A series of long galvanostatic electrolyses were carried out, at different current densities from 10 to 60 mA/cm^2, to monitor the concentration of H_2O_2 accumulated in a 0.050 M Na_2SO_4 solution at pH 3.0 for 360 min. In these trials, either an MC-C- or an N-MC-C-derived GDE was connected to a DSA plate. As can be seen in Figure 5a, with both types of GDE, a higher concentration was achieved as the electrolysis progressed, as a result of the effective ORR via reaction 1. However, the initially linear trends became curves after 120−180 min, which means that the processes that accounted for the H_2O_2 destruction gradually became more significant. The main ones among them were the following: (i) cathodic reduction via reaction 6, (ii) its oxidation at the anode surface, as the cell had one single compartment, and (iii) chemical decomposition and natural disproportionation in the bulk. In fact, a final plateau could be observed in some cases, especially at the highest current density of 60 mA/cm^2, which was reached once

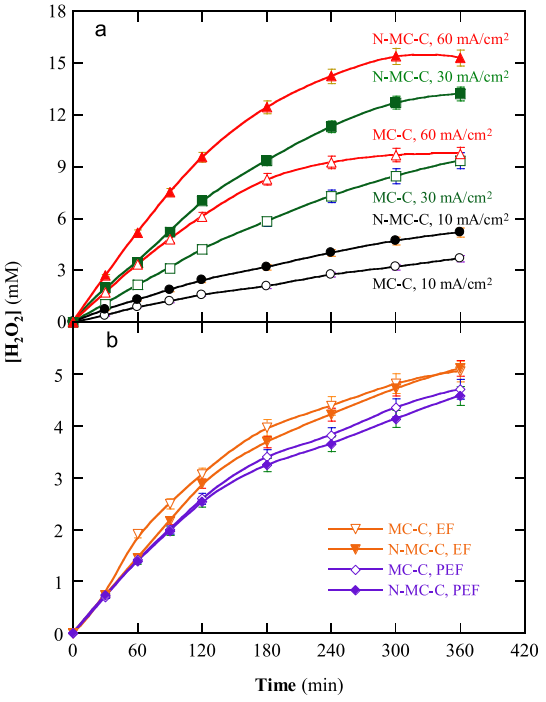

Figure 5. Evolution of H_2O_2 concentration during the electrolysis of 150 mL of 0.050 M Na_2SO_4 solutions at pH 3.0 and 25 °C, using a cell with the MC-C or N-MC-C cathode and a DSA plate as the anode at different current densities and an air flow rate of 36 L/h. Process: (a) EO-H_2O_2 and (b) EF with 0.50 mM Fe^{2+} and PEF with 0.50 mM Fe^{2+} and a 6 W UVA lamp.

https://dx.doi.org/10.1021/acssuschemeng.0c04294
ACS Sustainable Chem. Eng. 2020, 8, 14425−14440

the H_2O_2 formation and destruction rates became equal. At 360 min, the concentrations attained at 10, 30, and 60 mA/cm^2 were 3.68, 9.35, and 9.75 mM using MC-C and 5.20, 13.2, and 15.3 mM with N-MC-C, respectively. Therefore, the greatest values appeared in cells with the N-MC-C-derived GDE, regardless of the applied current density, which confirms the importance of the superficial N content and the corresponding N-functionalities described above. Furthermore, the difference was higher as the current density was increased (i.e., the curves with both GDEs were comparatively more separated), suggesting a relatively greater stability of N-MC-C under more aggressive conditions. In fact, using the MC-C-derived GDE, the H_2O_2 contents at 30 and 60 mA/cm^2 were very close, meaning that the stability range for that cathode was more limited. Such lower stability can be related to its structural characteristics, as discussed above, as a lower porosity and greater compactness constitute a barrier that oxygen gas tends to break in a rough manner.

A comparison with the reported values for H_2O_2 accumulation in similar setups that employed commercial C-PTFE GDEs allows concluding that the electrogeneration performance observed in this work is in the same range, in particular, in the case of the GDE prepared with N-MC-C. For example, 0.59 mM H_2O_2 (vs 2.00 mM in this work) was measured at 30 min in a 0.050 M Na_2SO_4 solution, pH 3.0, recirculated at a liquid flow rate of 4.4 L/min and electrolyzed at 30 mA/cm^2 in a pilot plant, whereas the content of 17 mM H_2O_2 was achieved after 360 min at 50 mA/cm^2 in a 2.5 L plant.[78] Moreover, the values represented in Figure 5a are much better than those typically attained with raw carbon-felt cathodes, which have also been employed in EF and PEF treatments.[5] These results corroborate that the electroactivity of the synthesized catalysts was high enough to accumulate H_2O_2, despite the partial selectivity observed from Figure 4. For a more accurate comparison with the literature, Table S2 summarizes the CE, H_2O_2 mass production rate, and H_2O_2 yield calculated for our best catalyst as well as for carbon electrocatalysts employed in GDEs for water treatment. Note that, despite the moderate efficiency of the new material to accumulate H_2O_2, the crucial finding of this work is that the electrogenerated amount is sufficient to promote the degradation of water pollutants (see subsections below).

The presence of Fe^{2+} in the solution (i.e., EF conditions) should cause a drastic reduction in the quantity of H_2O_2 accumulated because of its quick decomposition via Fenton's reaction 2. Indeed, this is verified in Figure 5b, which shows similar profiles regardless of the type of cathode when Fe^{2+} at a concentration of 0.50 mM was employed as a catalyst. The other conditions were analogous to those described in Figure 5a, at 30 mA/cm^2. Based on the almost identical trends to finally attain a value of ∼5.1 mM H_2O_2, and considering that the N-MC-C-derived GDE was proven to generate more H_2O_2 than the MC-C GDE in the absence of Fe^{2+} (Figure 5a), a greater $^{\bullet}OH$ production can be inferred. This should entail faster water decontamination, as will be discussed later. The result obtained in these EF systems is in good agreement with that previously reported with a commercial GDE in an analogous solution (<10 mM H_2O_2 at 30 mA/cm^2).[79] Similar experiments were made exposing solutions with the same composition to UVA photons (PEF conditions), which caused an additional reduction in the content of the oxidant accumulated at each electrolysis time until reaching ∼4.6 mM H_2O_2 at 360 min (Figure 5b). This is explained by the occurrence of photo-Fenton reaction 3, with optimum λ = 360 nm. The continuous Fe^{2+} photoinduced regeneration sustained Fenton's reaction 2, which otherwise would be mitigated due to the gradual conversion of Fe^{2+} into much less active species $[Fe(OH)]^{2+}$ (i.e., the main Fe(III) species at pH 3.0).[5]

The current efficiencies for all the trials depicted in Figure 5a,b, determined from eq 4, are illustrated in Figure S4a,b, respectively. In all cases, a loss of efficiency over time can be observed, in agreement with progressively lower H_2O_2 accumulation rate (i.e., the curvature appearance after some minutes in Figure 5 owing to parasitic reactions). In the absence of Fe^{2+} (Figure S4a), the maximum efficiency of ∼40% (reasonably good taking into account that the cell was undivided) corresponded to the treatment with N-MC-C at 10 mA/cm^2. It is worth noticing that upon increasing to 30 mA/cm^2, the efficiency profile was very similar, which is interesting in practice to promote a faster degradation. Therefore, this current density was selected as optimum for subsequent trials. When the current density was then doubled, the efficiency was almost halved, confirming the detrimental enhancement of parasitic destruction reactions (i.e., cathodic and anodic phenomena mentioned before). All the treatments with the MC-C-derived GDE were much less efficient (<25% during all the electrolysis). As expected from the practically overlapping H_2O_2 profiles found in EF and PEF (Figure 5a), Figure S4b evidences similar trends for the corresponding current efficiencies (always lower than 20%), with slightly higher values in EF assays.

Degradation of Acebutolol Using GDEs Prepared with the Synthesized Catalysts. For the dual purpose of assessing the viability of the new GDEs to foster the degradation of organic pollutants and confirming the superiority of the N-MC-C electrocatalyst, solutions containing 0.046 mM of the β-blocker acebutolol and 0.050 M Na_2SO_4 at pH 3.0 were electrolyzed at the optimized current density (30 mA/cm^2). In Figure 6a, the drug concentration decays under electro-oxidation (EO-H_2O_2) conditions with each GDE. The degradation was quite slow in both cases, ending in moderate removal of 35 and 51% at 180 min using the MC-C- and N-MC-C-derived GDE, respectively. As H_2O_2 behaves as a rather mild oxidant in front of aromatic structures like that exhibited by acebutolol, within the concentration ranges as that discussed in Figure 5a,[6] the partial drug disappearance can be attributed to the action of hydroxyl radicals M($^{\bullet}OH$) formed on the anode (M) surface from reaction 13.[40,48] The data could not be fitted well considering a simple kinetic model, thus suggesting a larger complexity due to the influence of reaction products.

$$M + H_2O \rightarrow M(^{\bullet}OH) + H^+ + e^- \quad (13)$$

The degradation was drastically upgraded in the presence of 0.50 mM Fe^{2+} and UVA photons under PEF conditions, as evidenced in Figure 6b. The use of the two DSA/GDE cells led to 97 and 100% acebutolol removal in only 20 min using the MC-C and N-MC-C electrocatalysts, respectively. Such significant acceleration of concentration decays was pre-eminently favored by the generation of $^{\bullet}OH$ upon fast decomposition of H_2O_2 via Fenton's reaction 2, which confirms the explanation given on the time course of H_2O_2 (Figure 5b). The effective $^{\bullet}OH$ production was ensured by the continuous Fe(III) photoreduction from reaction 3, which yielded additional amounts of $^{\bullet}OH$ and regenerated the Fe^{2+}. The replacement of the RuO_2-based anode by BDD had a

https://dx.doi.org/10.1021/acssuschemeng.0c04294
ACS Sustainable Chem. Eng. 2020, 8, 14425−14440

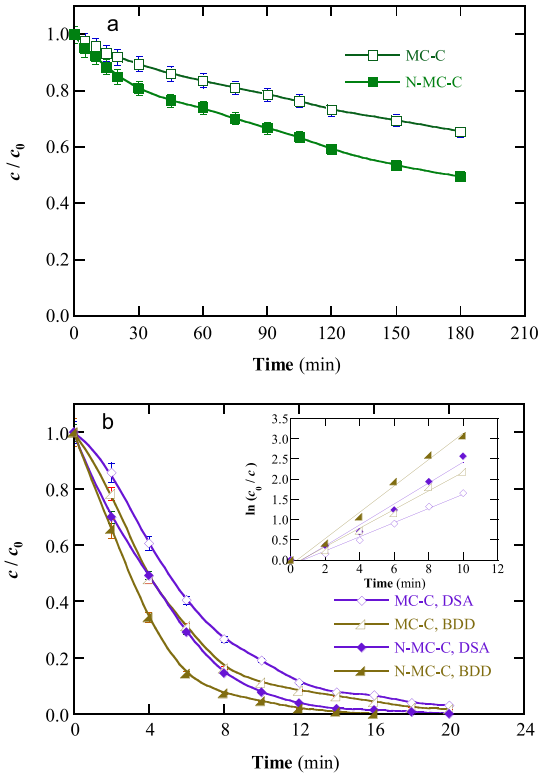

Figure 6. Time course of acebutolol concentration during the treatment of 150 mL of solutions with 0.046 mM drug and 0.050 M Na_2SO_4 at pH 3.0 and 25 °C, using a cell with the MC-C or N-MC-C cathode at a current density of 30 mA/cm^2 and an air flow rate of 36 L/h. Process: (a) EO-H_2O_2 with DSA and (b) PEF with 0.50 mM Fe^{2+}, a 6 W UVA lamp, and DSA or BDD as the anode. In (b), the inset panel presents the corresponding pseudo-first-order kinetic analysis.

positive influence on the destruction of the pollutant, being more evident in the system with N-MC-C, as complete disappearance was observed at 16 min. Using MC-C, almost no change in the degradation percentage (98%) was achieved, but the initial concentration decay became quicker. This is clear in the inset of Figure 6b, which depicts the excellent linear fitting (R^2 > 0.990) resulting from a pseudo-first-order kinetic analysis of all decays of the main figure. The pseudo-first-order rate constant (k_1) increased from 0.1748 to 0.2296 min^{-1} when the anode was changed to BDD in the system with MC-C. Accordingly, higher k_1-values were determined using N-MC-C, namely, 0.2583 and 0.3258 min^{-1} with DSA and BDD, respectively. The enhancement achieved with the BDD anode is associated with the physisorbed nature of M(•OH) produced from reaction 13, which makes the radicals more reactive with organic molecules approaching its surface.[48] However, it is clear that the main factors affecting the drug degradation were those related with the Fenton's reactivity, as can be deduced when comparing Figure 6a,b. Among such factors, the benefit of the higher H_2O_2 electrogeneration with N-MC-C stands out.

The performance of our biomass-derived GDEs is comparable to that reported for GDEs prepared with carbon cloth coated with commercial carbon black. For example, the treatment of β-blocker atenolol in 0.050 M Na_2SO_4 at pH 3.0 by PEF at 16.7 mA/cm^2 allowed the total drug removal in 30–35 min, with k_1 = 0.05 min^{-1}, and thus is of the same order of magnitude.[80]

Figure 7 highlights the time course of normalized TOC content with electrolysis time during the PEF assays of Figure 6b. Unlike that observed in the previous HPLC analysis, the effect of the anode nature was crucial to upgrade the mineralization of the solutions, which initially contained 10 mg/L TOC. Partial TOC abatements were obtained with DSA, attaining 71 and 76% at 360 min using MC-C and N-MC-C, respectively. A much greater decontamination was feasible upon use of the BDD anode, with final values of 91 and 97%. In all these systems, the effective generation of •OH in the bulk sustained by reaction 3 undoubtedly contributed to the gradual degradation of reaction products. However, this was insufficient because it is known that the aromatic molecules are transformed into very refractory aliphatic products and their complexes with Fe(III) resist quite well the attack of •OH.[3,4] Therefore, UVA photons played an additional role, allowing the photodecarboxylation of such stable complexes.

$$[Fe(OOCR)]^{2+} + h\nu \rightarrow Fe^{2+} + R^{\bullet} + CO_2 \quad (14)$$

As inferred from both PEF trials with DSA, the degradation power of •OH and UVA light was still limited, and hence M(•OH) formed at BDD favored the electrocatalytic destruction of the refractory molecules. As a result, the combination of the most effective anode and cathode yielded the greater mineralization. Note that TOC decays reported for acebutolol solutions through other advanced oxidation processes were lower, as in the case of photocatalysis with TiO_2 with 75% mineralization at 240 min.[81]

The following overall mineralization reaction can be proposed based on the determination of inorganic ions, as discussed below[5]:

$$C_{18}H_{28}N_2O_4 + 32H_2O \rightarrow 18CO_2 + 2NH_4^+ + 84H^+ + 86e^- \quad (15)$$

From eq 5, in which the total number of electrons involved was n = 86, the MCE values calculated at a given electrolysis time for the assays in Figure 7 are represented in Figure S5a. The most efficient process was PEF with the BDD/GDE cell using N-MC-C, in agreement with the effective TOC removal in that system. Nonetheless, the fact that the maximum MCE was <15% reflects the high refractoriness of the pollutant and its derivatives. As the treatments progressed, a loss of efficiency was observed, meaning that the organic structures and

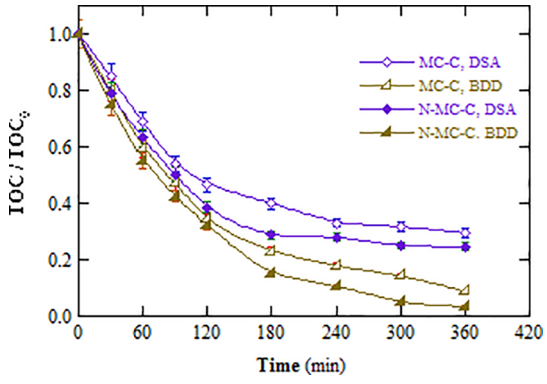

Figure 7. Change in the normalized TOC with electrolysis time for the PEF trials shown in Figure 6b.

https://dx.doi.org/10.1021/acssuschemeng.0c04294
ACS Sustainable Chem. Eng. 2020, 8, 14425−14440

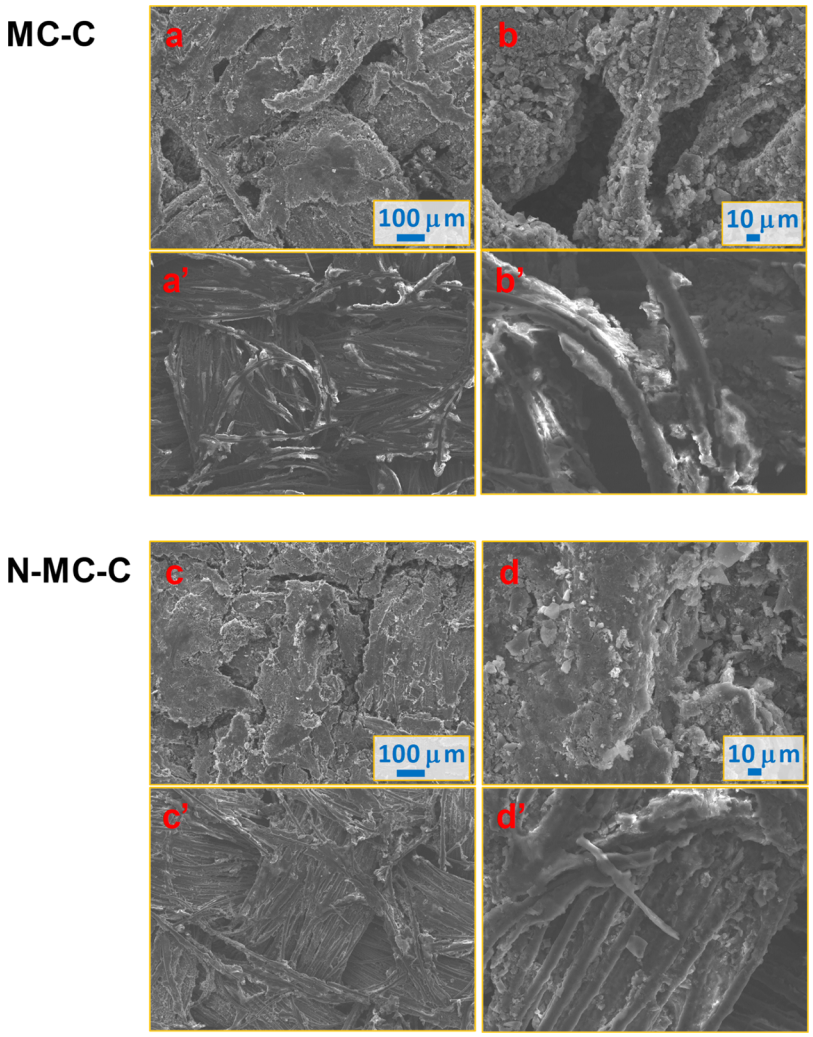

Figure 8. SEM images of GDEs prepared with chitosan-based electrocatalysts. (a−d) Fresh and (a′−d′) used. Magnification: (a,a′,c,c′) 100× and (b,b′,d,d′) 500×. The used GDEs were those collected at the end of the PEF treatments with DSA described in Figure 7.

complexes formed were more resistant to $^{\bullet}OH$, M($^{\bullet}OH$), and UVA photons than the target pollutant and its primary intermediates. In addition, the side reactions that wasted the radicals and photons occurred to a greater extent as the number of available organic molecules decreased. These two phenomena with a negative impact on the process efficiency were also detrimental in terms of energy consumption. The EC_{TOC} values calculated from eq 6 and represented in Figure 6b were higher in trials with BDD, which is mainly explained by the much greater E_{cell} as compared to those with the RuO_2-based anode (15.5 vs 8.0 V, regardless of the GDE). Note that these energy consumptions are purely electrolytic. If the lamp consumption is added (i.e., the term $E_{cell}I$ in eq 6 is replaced by the lamp power to determine $(EC)_{photo}$),[82] the EC_{TOC} values increase up to ∼30 and ∼36 kW h/g TOC using BDD and DSA, respectively. In practice, natural sunlight can be used instead of artificial UVA light, thus avoiding the large contribution of $(EC)_{photo}$.

In Figure 8a−d, the SEM images of GDEs prepared with both chitosan-based electrocatalysts can be seen at two different magnifications. A good surface coverage of carbon cloth was obtained with MC-C and N-MC-C, with no evidence of exposed carbon fibers. This is attributed to the good spraying procedure, giving rise to several layers, followed by hot pressing. Some gaps can be appreciated, which are better identified at the highest magnification (Figure 8b,d). These macropores favored the mass transport rate of O_2 toward the catalytic sites.[5] Amorphous particles with dimensions of some microns appear in both types of GDE, as is typical for C-PTFE GDEs. Some of them formed clusters wrapped around the fibers (Figure 8b). PTFE, recognized as the white spots, was spread over the surface, conferring sufficient hydrophobicity to the materials. Note that no flooding of the GDEs was observed during the trials of this work. The GDEs used in PEF treatments with DSA described in Figure 7 were collected at the end of the electrolyses. The corresponding SEM analysis (Figure 8a′−d′) at the same magnifications mainly show smoother surfaces without clear distinction of carbon particles and, more importantly, the obvious presence of uncoated or partially coated fibers. This phenomenon was more evident in the cathode prepared with MC-C, which can be directly explained from its aforementioned lower stability. Oxygen gas is forced through its compact structure, causing a partial disintegration. However, this did not impede reuse of all the GDEs for several consecutive runs without any substantial loss of performance related to H_2O_2 production and degradation ability.

https://dx.doi.org/10.1021/acssuschemeng.0c04294
ACS Sustainable Chem. Eng. 2020, 8, 14425−14440

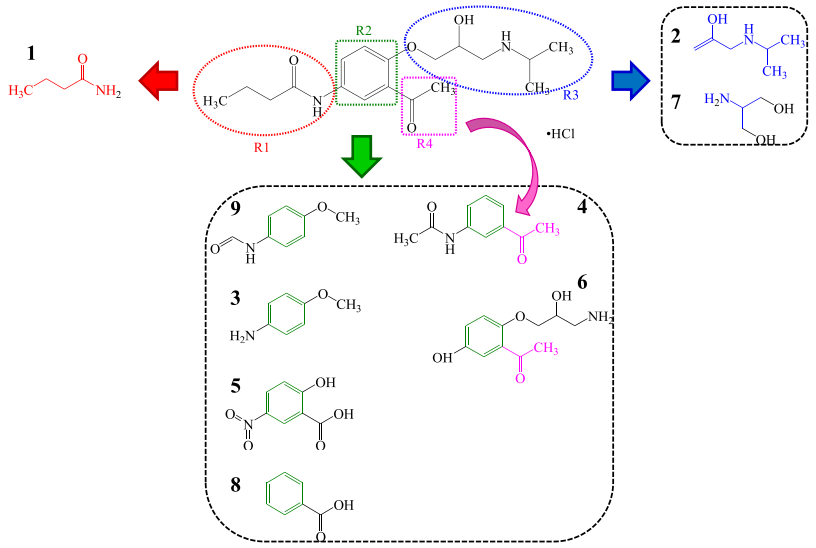

Figure 9. Primary products of acebutolol during PEF treatment with chitosan-derived electrocatalysts.

Reaction Products Identified during the PEF Treatment of Acebutolol Solutions. In the previous subsection, the TOC−time and MCE−time profiles have been justified on the basis of the different reactivities of the reaction products. To demonstrate this, a 0.046 mM acebutolol solution with 0.050 M Na_2SO_4 and 0.50 mM Fe^{2+} at pH 3.0 was treated by PEF for 60 min, using a cell with the RuO_2-based anode connected to a GDE made with a N-MC-C catalyst, at 30 mA/cm^2. Samples collected at 10 and 60 min and analyzed by GC/MS revealed the presence of six aromatic and three nitrogenated aliphatic compounds, whose characteristics are summarized in Table S3. In Figure 9, the generation of these molecules is proposed considering the modification of parts R1, R2, R3, and R4 distinguished in acebutolol. Some authors detected a product similar to **2**, but hydroxylated in C1 position, when acebutolol solutions were treated by droplet-assisted heterogeneous EF.[83] They also identified a structure close to **6** but keeping R1 and another one like **7** but nonhydroxylated.

Most of these nine products were expected to be gradually hydroxylated.[5] Therefore, the evolution of the concentration of short-chain linear carboxylic acids during the same kind of PEF treatment was investigated. Figure 10 evidences the trends of oxalic acid, whose peak was found at a retention time of 7.0 min, and of oxamic acid, which appeared at 9.8 min. The former attained a maximum concentration of 1.75 mg/L at 30 min, quickly decaying to finally disappear at 120 min. Oxalic acid is a typical end-organic product from aromatic pollutants, which explains the reason for it being the main accumulated carboxylic acid.[51] The high photoactivity of its complexed form under UVA light according to reaction 14 justifies its total degradation in PEF. In contrast, oxamic acid was only formed from larger N-structures, reaching a lower content of 1.05 mg/L at 60 min. Moreover, as it formed much less photoactive complexes,[51] it persisted in the solution during the entire electrolysis. The presence of both acids as acebutolol is degraded has also been reported elsewhere.[83]

The inorganic ions generated in PEF treatment from the heteroatoms contained in the drug were determined as well. A more concentrated acebutolol solution (i.e., 0.092 mM) was employed in order to facilitate the quantification. Neither nitrite nor nitrate was identified, NH_4^+ being the only dissolved

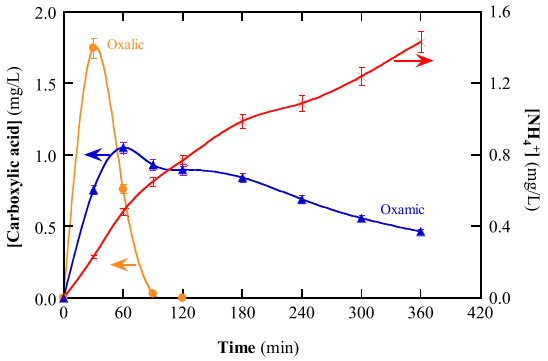

Figure 10. Evolution of the concentration of aliphatic carboxylic acids during the PEF treatment of 0.046 mM acebutolol solutions with 0.050 M Na_2SO_4 and 0.50 mM Fe^{2+}, as well as NH_4^+ content accumulated during an analogous treatment but using 0.092 mM drug and 0.020 M Na_2SO_4 instead. Conditions: cell with the N-MC-C cathode (fed with air at 36 L/h) and the RuO_2-based anode, containing 150 mL of solutions at pH 3.0 and 25 °C exposed to a 6 W UVA lamp and electrolyzed at 30 mA/cm^2.

nitrogenated ion detected, thus corroborating the validity of mineralization reaction 15. The ammonium content increased all the time, as the organic N-structures were degraded, attaining 1.43 mg/L at 360 min. This cation was also the main nitrogenated ion found during the degradation of other N-aromatic pollutants by Fenton-based electrochemical processes.[70] A nitrogen balance after normalizing the acebutolol content suggests that the treated solutions contained ∼50% of initial dissolved nitrogen, most of it corresponding to NH_4^+. This means that some N-containing gases were released during the PEF treatment of acebutolol.

CONCLUSIONS

This work reports the successful synthesis and characterization of a potentially cheaper and more eco-friendly material to electrogenerate sufficient amounts of H_2O_2 for its direct application in Fenton-based electrochemical water treatment. Chitosan was considered as the raw material for the preparation of N-doped carbon. It was observed that the addition of 1,10-phenanthroline as a coreactant during the

https://dx.doi.org/10.1021/acssuschemeng.0c04294
ACS Sustainable Chem. Eng. 2020, 8, 14425−14440

pyrolysis treatments conferred better textural properties and surface N-functionalization than the sole chitosan. LSV at RRDE highlighted the higher catalytic activity of N-MC-C, in terms of $E_{1/2}$. GDEs prepared with N-MC-C showed H_2O_2 yields in the same range attainable with commercial GDE. The degradation of 0.046 mM acebutolol solutions was made with the N-MC-C-derived GDE coupled to a RuO_2-based anode in an electrochemical cell at pH 3.0. The PEF assays in such cell resulted in fast and complete drug removal. The use of BDD instead of DSA had a positive influence on the decontamination, as almost complete TOC removal was achieved at the end of electrolysis. GC/MS analysis clarified the main aromatic and aliphatic products formed during the mineralization process. Short-chain linear carboxylic acids such as oxalic and oxamic acids were generated as final organic compounds, whereas NH_4^+ was the main ion.

■ ASSOCIATED CONTENT

Supporting Information

The Supporting Information is available free of charge at https://pubs.acs.org/doi/10.1021/acssuschemeng.0c04294.

UV−vis, Raman, and XPS survey spectra; CE; MCE; XPS speciation; performance of selected commercial and noncommercial electrocatalysts; and products detected by GC/MS upon acebutolol degradation (PDF)

■ AUTHOR INFORMATION

Corresponding Authors

Christian Durante − *Department of Chemical Sciences, University of Padua, 35131 Padova, Italy;* orcid.org/0000-0002-8764-1219; Phone: +39 0498275112; Email: christian.durante@unipd.it; Fax: +39 0498275829

Ignasi Sirés − *Laboratori d'Electroquímica dels Materials i del Medi Ambient, Departament de Química Física, Facultat de Química, Universitat de Barcelona, 08028 Barcelona, Spain;* orcid.org/0000-0001-5508-1774; Phone: +34 934039240; Email: i.sires@ub.edu; Fax: +34 934021231

Authors

Giorgia Daniel − *Department of Chemical Sciences, University of Padua, 35131 Padova, Italy*

Yanyu Zhang − *Laboratori d'Electroquímica dels Materials i del Medi Ambient, Departament de Química Física, Facultat de Química, Universitat de Barcelona, 08028 Barcelona, Spain; Department of Municipal and Environmental Engineering, Beijing Key Laboratory of Aqueous Typical Pollutants Control and Water Quality Safeguard, Beijing Jiaotong University, 100044 Beijing, China*

Sonia Lanzalaco − *Departament d'Enginyeria Química, EEBE, Universitat Politècnica de Catalunya, 08019 Barcelona, Spain*

Federico Brombin − *Department of Chemical Sciences, University of Padua, 35131 Padova, Italy*

Tomasz Kosmala − *Department of Chemical Sciences, University of Padua, 35131 Padova, Italy;* orcid.org/0000-0002-0026-8205

Gaetano Granozzi − *Department of Chemical Sciences, University of Padua, 35131 Padova, Italy;* orcid.org/0000-0002-9509-6142

Aimin Wang − *Department of Municipal and Environmental Engineering, Beijing Key Laboratory of Aqueous Typical Pollutants Control and Water Quality Safeguard, Beijing Jiaotong University, 100044 Beijing, China*

Enric Brillas − *Laboratori d'Electroquímica dels Materials i del Medi Ambient, Departament de Química Física, Facultat de Química, Universitat de Barcelona, 08028 Barcelona, Spain*

Complete contact information is available at: https://pubs.acs.org/10.1021/acssuschemeng.0c04294

Author Contributions

$^{\perp}$G.D. and Y.Z. contributed equally to this work.

Notes

The authors declare no competing financial interest.

■ ACKNOWLEDGMENTS

The authors kindly acknowledge support from projects DOR2018 (University of Padova), CTQ2016-78616-R (AEI/FEDER, EU), and PID2019-109291RB-I00 (AEI, Spain), as well as the PhD scholarship awarded to Y.Z. (State Scholarship Fund, CSC, China).

■ REFERENCES

(1) Guo, X.; Lin, S.; Gu, J.; Zhang, S.; Chen, Z.; Huang, S. Simultaneously achieving high activity and selectivity toward two-electron O_2 electroreduction: The power of single-atom catalysts. *ACS Catal.* **2019**, *9*, 11042−11054.

(2) Rocha, R. S.; Silva, F. L.; Valim, R. B.; Barros, W. R. P.; Steter, J. R.; Bertazzoli, R.; Lanza, M. R. V. Effect of Fe^{2+} on the degradation of the pesticide profenofos by electrogenerated H_2O_2. *J. Electroanal. Chem.* **2016**, *783*, 100−105.

(3) Ye, Z.; Guelfi, D. R. V.; Álvarez, G.; Alcaide, F.; Brillas, E.; Sirés, I. Enhanced electrocatalytic production of H_2O_2 at Co-based air-diffusion cathodes for the photoelectro-Fenton treatment of bronopol. *Appl. Catal., B* **2019**, *247*, 191−199.

(4) Alcaide, F.; Álvarez, G.; Guelfi, D. R. V.; Brillas, E.; Sirés, I. A stable CoSP/MWCNTs air-diffusion cathode for the photoelectro-Fenton degradation of organic pollutants at pre-pilot scale. *Chem. Eng. J.* **2020**, *379*, 122417.

(5) Brillas, E.; Sirés, I.; Oturan, M. A. Electro-Fenton process and related electrochemical technologies based on Fenton's reaction chemistry. *Chem. Rev.* **2009**, *109*, 6570−6631.

(6) Borghei, M.; Lehtonen, J.; Liu, L.; Rojas, O. J. Advanced biomass-derived electrocatalysts for the oxygen reduction reaction. *Adv. Mater.* **2018**, *30*, 1703691.

(7) Chai, G.-L.; Hou, Z.; Ikeda, T.; Terakura, K. Two-electron oxygen reduction on carbon materials catalysts: Mechanisms and active sites. *J. Phys. Chem. C* **2017**, *121*, 14524−14533.

(8) Chen, S.; Chen, Z.; Siahrostami, S.; Kim, T. R.; Nordlund, D.; Sokaras, D.; Nowak, S.; To, J. W. F.; Higgins, D.; Sinclair, R.; Nørskov, J. K.; Jaramillo, T. F.; Bao, Z. Defective carbon-based materials for the electrochemical synthesis of hydrogen peroxide. *ACS Sustainable Chem. Eng.* **2018**, *6*, 311−317.

(9) Čolić, V.; Yang, S.; Révay, Z.; Stephens, I. E. L.; Chorkendorff, I. Carbon catalysts for electrochemical hydrogen peroxide production in acidic media. *Electrochim. Acta* **2018**, *272*, 192−202.

(10) Sun, Y.; Sinev, I.; Ju, W.; Bergmann, A.; Dresp, S.; Kühl, S.; Spöri, C.; Schmies, H.; Wang, H.; Bernsmeier, D.; Paul, B.; Schmack, R.; Kraehnert, R.; Roldan Cuenya, B.; Strasser, P. Efficient electrochemical hydrogen peroxide production from molecular oxygen on nitrogen-doped mesoporous carbon catalysts. *ACS Catal.* **2018**, *8*, 2844−2856.

(11) Choi, C. H.; Kim, M.; Kwon, H. C.; Cho, S. J.; Yun, S.; Kim, H.-T.; Mayrhofer, K. J. J.; Kim, H.; Choi, M. Tuning selectivity of electrochemical reactions by atomically dispersed platinum catalyst. *Nat. Commun.* **2016**, *7*, 10922.

(12) Perazzolo, V.; Durante, C.; Pilot, R.; Paduano, A.; Zheng, J.; Rizzi, G. A.; Martucci, A.; Granozzi, G.; Gennaro, A. Nitrogen and sulfur doped mesoporous carbon as metal-free electrocatalysts for the in situ production of hydrogen peroxide. *Carbon* **2015**, *95*, 949−963.

(13) Perazzolo, V.; Durante, C.; Gennaro, A. Nitrogen and sulfur doped mesoporous carbon cathodes for water treatment. *J. Electroanal. Chem.* **2016**, *782*, 264−269.
(14) Roldán, L.; Truong-Phuoc, L.; Ansón-Casaos, A.; Pham-Huu, C.; García-Bordejé, E. Mesoporous carbon doped with N,S heteroatoms prepared by one-pot auto-assembly of molecular precursor for electrocatalytic hydrogen peroxide synthesis. *Catal. Today* **2018**, *301*, 2−10.
(15) Favaro, M.; Perini, L.; Agnoli, S.; Durante, C.; Granozzi, G.; Gennaro, A. Electrochemical behavior of N and Ar implanted highly oriented pyrolytic graphite substrates and activity toward oxygen reduction reaction. *Electrochim. Acta* **2013**, *88*, 477−487.
(16) Xing, T.; Sunarso, J.; Yang, W.; Yin, Y.; Glushenkov, A. M.; Li, L. H.; Howlett, P. C.; Chen, Y. Ball milling: a green mechanochemical approach for synthesis of nitrogen doped carbon nanoparticles. *Nanoscale* **2013**, *5*, 7970−7976.
(17) Tuci, G.; Zafferoni, C.; Rossin, A.; Milella, A.; Luconi, L.; Innocenti, M.; Truong Phuoc, L.; Duong-Viet, C.; Pham-Huu, C.; Giambastiani, G. Chemically functionalized carbon nanotubes with pyridine groups as easily tunable N-decorated nanomaterials for the oxygen reduction reaction in alkaline medium. *Chem. Mater.* **2014**, *26*, 3460−3470.
(18) Kabir, S.; Artyushkova, K.; Serov, A.; Atanassov, P. Role of nitrogen moieties in N-doped 3D-graphene nanosheets for oxygen electroreduction in acidic and alkaline media. *ACS Appl. Mater. Interfaces* **2018**, *10*, 11623−11632.
(19) Brandiele, R.; Durante, C.; Zerbetto, M.; Vicentini, N.; Kosmala, T.; Badocco, D.; Pastore, P.; Rizzi, G. A.; Isse, A. A.; Gennaro, A. Probing the correlation between Pt-support interaction and oxygen reduction reaction activity in mesoporous carbon materials modified with Pt-N active sites. *Electrochim. Acta* **2018**, *277*, 287−300.
(20) Yang, W.; Zhou, M.; Liang, L. Highly efficient in-situ metal-free electrochemical advanced oxidation process using graphite felt modified with N-doped graphene. *Chem. Eng. J.* **2018**, *338*, 700−708.
(21) Yang, W.; Zhou, M.; Oturan, N.; Li, Y.; Su, P.; Oturan, M. A. Enhanced activation of hydrogen peroxide using nitrogen doped graphene for effective removal of herbicide 2,4-D from water by iron-free electrochemical advanced oxidation. *Electrochim. Acta* **2019**, *297*, 582−592.
(22) Iglesias, D.; Giuliani, A.; Melchionna, M.; Marchesan, S.; Criado, A.; Nasi, L.; Bevilacqua, M.; Tavagnacco, C.; Vizza, F.; Prato, M.; Fornasiero, P. N-doped graphitized carbon nanohorns as a forefront electrocatalyst in highly selective O2 reduction to H2O2. *Chem* **2018**, *4*, 106−123.
(23) Bi, Z.; Kong, Q.; Cao, Y.; Sun, G.; Su, F.; Wei, X.; Li, X.; Ahmad, A.; Xie, L.; Chen, C.-M. Biomass-derived porous carbon materials with different dimensions for supercapacitor electrodes: a review. *J. Mater. Chem. A* **2019**, *7*, 16028−16045.
(24) Antolini, E. Nitrogen-doped carbons by sustainable N- and C-containing natural resources as nonprecious catalysts and catalyst supports for low temperature fuel cells. *Renewable Sustainable Energy Rev.* **2016**, *58*, 34−51.
(25) Liu, F.; Liu, L.; Li, X.; Zeng, J.; Du, L.; Liao, S. Nitrogen self-doped carbon nanoparticles derived from spiral seaweeds for oxygen reduction reaction. *RSC Adv.* **2016**, *6*, 27535−27541.
(26) Chen, Y.; Wang, M.; Tian, M.; Zhu, Y.; Wei, X.; Jiang, T.; Gao, S. An innovative electro-Fenton degradation system self-powered by triboelectric nanogenerator using biomass-derived carbon materials as cathode catalyst. *Nano Energy* **2017**, *42*, 314−321.
(27) Yang, Y.; He, F.; Shen, Y.; Chen, X.; Mei, H.; Liu, S.; Zhang, Y. A biomass derived N/C-catalyst for the electrochemical production of hydrogen peroxide. *Chem. Commun.* **2017**, *53*, 9994−9997.
(28) Daniel, G.; Foltran, E.; Brandiele, R.; Nodari, L.; Pilot, R.; Menna, E.; Rizzi, G. A.; Ahmed Isse, A.; Durante, C.; Gennaro, A. Platinum-free electrocatalysts for oxygen reduction reaction: Fe-N_x modified mesoporous carbon prepared from biosources. *J. Power Sources* **2018**, *402*, 434−446.
(29) Kim, M.-J.; Park, J. E.; Kim, S.; Lim, M. S.; Jin, A.; Kim, O.-H.; Kim, M. J.; Lee, K.-S.; Kim, J.; Kim, S.-S.; Cho, Y.-H.; Sung, Y.-E. Biomass-derived air cathode materials: Pore-controlled S,N-co-doped carbon for fuel cells and metal−air batteries. *ACS Catal.* **2019**, *9*, 3389−3398.
(30) Tian, M.; Zhu, Y.; Zhang, D.; Wang, M.; Chen, Y.; Yang, Y.; Gao, S. Pyrrolic-nitrogen-rich biomass-derived catalyst for sustainable degradation of organic pollutant via a self-powered electro-Fenton process. *Nano Energy* **2019**, *64*, 103940.
(31) Wu, X.; Chen, K.; Lin, Z.; Zhang, Y.; Meng, H. Nitrogen doped graphitic carbon from biomass as non noble metal catalyst for oxygen reduction reaction. *Mater. Today Energy* **2019**, *13*, 100−108.
(32) Jia, N.; Yang, T.; Shi, S.; Chen, X.; An, Z.; Chen, Y.; Yin, S.; Chen, P. N,F-codoped carbon nanocages: An efficient electrocatalyst for hydrogen peroxide electroproduction in alkaline and acidic solutions. *ACS Sustainable Chem. Eng.* **2020**, *8*, 2883−2891.
(33) Le, T. X. H.; Bechelany, M.; Lacour, S.; Oturan, N.; Oturan, M. A.; Cretin, M. High removal efficiency of dye pollutants by electro-Fenton process using a graphene based cathode. *Carbon* **2015**, *94*, 1003−1011.
(34) Castañeda, L. F.; Walsh, F. C.; Nava, J. L.; Ponce de León, C. Graphite felt as a versatile electrode material: Properties, reaction environment, performance and applications. *Electrochim. Acta* **2017**, *258*, 1115−1139.
(35) Yu, F.; Chen, Y.; Ma, H. Ultrahigh yield of hydrogen peroxide and effective diclofenac degradation on a graphite felt cathode loaded with CNTs and carbon black: an electro-generation mechanism and a degradation pathway. *New J. Chem.* **2018**, *42*, 4485−4494.
(36) Ye, Z.; Brillas, E.; Centellas, F.; Cabot, P. L.; Sirés, I. Electro-Fenton process at mild pH using Fe(III)-EDDS as soluble catalyst and carbon felt as cathode. *Appl. Catal., B* **2019**, *257*, 117907.
(37) Scialdone, O.; Galia, A.; Gattuso, C.; Sabatino, S.; Schiavo, B. Effect of air pressure on the electro-generation of H_2O_2 and the abatement of organic pollutants in water by electro-Fenton process. *Electrochim. Acta* **2015**, *182*, 775−780.
(38) Zhou, W.; Meng, X.; Gao, J.; Alshawabkeh, A. N. Hydrogen peroxide generation from O_2 electroreduction for environmental remediation: A state-of-the-art review. *Chemosphere* **2019**, *225*, 588−607.
(39) Coria, G.; Pérez, T.; Sirés, I.; Brillas, E.; Nava, J. L. Abatement of the antibiotic levofloxacin in a solar photoelectro-Fenton flow plant: Modeling the dissolved organic carbon concentration-time relationship. *Chemosphere* **2018**, *198*, 174−181.
(40) Galia, A.; Lanzalaco, S.; Sabatino, M. A.; Dispenza, C.; Scialdone, O.; Sirés, I. Crosslinking of poly(vinylpyrrolidone) activated by electrogenerated hydroxyl radicals: a first step towards a simple and cheap synthetic route of nanogel vectors. *Electrochem. Commun.* **2016**, *62*, 64−68.
(41) Lanzalaco, S.; Sirés, I.; Sabatino, M. A.; Dispenza, C.; Scialdone, O.; Galia, A. Synthesis of polymer nanogels by electro-Fenton process: investigation of the effect of main operation parameters. *Electrochim. Acta* **2017**, *246*, 812−822.
(42) Ding, P.; Cui, L.; Li, D.; Jing, W. Innovative dual-compartment flow reactor coupled with a gas diffusion electrode for in situ generation of H_2O_2. *Ind. Eng. Chem. Res.* **2019**, *58*, 6925−6932.
(43) Zhang, H.; Li, Y.; Zhao, Y.; Li, G.; Zhang, F. Carbon black oxidized by air calcination for enhanced H_2O_2 generation and effective organics degradation. *ACS Appl. Mater. Interfaces* **2019**, *11*, 27846−27853.
(44) Zhang, Q.; Zhou, M.; Ren, G.; Li, Y.; Li, Y.; Du, X. Highly efficient electrosynthesis of hydrogen peroxide on a superhydrophobic three-phase interface by natural air diffusion. *Nature Commun.* **2020**, *11*, 1731.
(45) Gendel, Y.; Roth, H.; Rommerskirchen, A.; David, O.; Wessling, M. A microtubular all CNT gas diffusion electrode. *Electrochem. Commun.* **2014**, *46*, 44−47.
(46) Mousset, E.; Ko, Z. T.; Syafiq, M.; Wang, Z.; Lefebvre, O. Electrocatalytic activity enhancement of a graphene ink-coated carbon

cloth cathode for oxidative treatment. *Electrochim. Acta* **2016**, *222*, 1628−1641.
(47) Kolyagin, G. A.; Kornienko, G. V.; Kornienko, V. L.; Ponomarenko, I. V. Electrochemical reduction of oxygen to hydrogen peroxide in a gas-diffusion electrode based on mesoporous carbon. *Russ. J. Appl. Chem.* **2017**, *90*, 1143−1147.
(48) Martínez-Huitle, C. A.; Rodrigo, M. A.; Sirés, I.; Scialdone, O. Single and coupled electrochemical processes and reactors for the abatement of organic water pollutants: a critical review. *Chem. Rev.* **2015**, *115*, 13362−13407.
(49) Yang, W.; Zhou, M.; Oturan, N.; Li, Y.; Oturan, M. A. Electrocatalytic destruction of pharmaceutical imatinib by electro-Fenton process with graphene-based cathode. *Electrochim. Acta* **2019**, *305*, 285−294.
(50) Ye, Z.; Padilla, J. A.; Xuriguera, E.; Beltran, J. L.; Alcaide, F.; Brillas, E.; Sirés, I. A highly stable metal-organic framework-engineered FeS_2/C nanocatalyst for heterogeneous electro-Fenton treatment: Validation in wastewater at mild pH. *Environ. Sci. Technol.* **2020**, *54*, 4664−4674.
(51) Zhou, M.; Oturan, M. A.; Sirés, I. *Electro-Fenton Process: New Trends and Scale-Up*; Springer Nature; Singapore, 2018.
(52) Brillas, E. A review on the photoelectro-Fenton process as efficient electrochemical advanced oxidation for wastewater remediation. Treatment with UV light, sunlight, and coupling with conventional and other photo-assisted advanced technologies. *Chemosphere* **2020**, *250*, 126198.
(53) Wen, Z.; Wang, A.; Zhang, Y.; Ren, S.; Tian, X.; Li, J. Mineralization of cefoperazone in acid medium by the microwave discharge electrodeless lamp irradiated photoelectro-Fenton using a RuO_2/Ti or boron-doped diamond anode. *J. Hazard. Mater.* **2019**, *374*, 186−194.
(54) Zhang, Y.; Wang, A.; Ren, S.; Wen, Z.; Tian, X.; Li, D.; Li, J. Effect of surface properties of activated carbon fiber cathode on mineralization of antibiotic cefalexin by electro-Fenton and photo-electro-Fenton treatments: Mineralization, kinetics and oxidation products. *Chemosphere* **2019**, *221*, 423−432.
(55) Liu, T.; Wang, K.; Song, S.; Brouzgou, A.; Tsiakaras, P.; Wang, Y. New electro-Fenton gas diffusion cathode based on nitrogen-doped graphene@carbon nanotube composite materials. *Electrochim. Acta* **2016**, *194*, 228−238.
(56) Zhu, Y.; Qiu, S.; Deng, F.; Ma, F.; Zheng, Y. Degradation of sulfathiazole by electro-Fenton using a nitrogen-doped cathode and a BDD anode: Insight into the H_2O_2 generation and radical oxidation. *Sci. Total Environ.* **2020**, *722*, 137853.
(57) Liao, M. J.; Wang, Y. L.; Li, S. S.; Li, J. F.; Chen, P. Electrocatalyst derived from abundant biomass and its excellent activity for in situ H_2O_2 production. *ChemElectroChem* **2019**, *6*, 4877−4884.
(58) Pujol, A. A.; León, I.; Cárdenas, J.; Sepúlveda-Guzmán, S.; Manríquez, J.; Sirés, I.; Bustos, E. Degradation of phenols by heterogeneous electro-Fenton with a Fe_3O_4-chitosan composite and a boron-doped diamond anode. *Electrochim. Acta* **2020**, *337*, 135784.
(59) El Knidri, H.; Belaabed, R.; Addaou, A.; Laajeb, A.; Lahsini, A. Extraction, chemical modification and characterization of chitin and chitosan. *Int. J. Biol. Macromol.* **2018**, *120*, 1181−1189.
(60) Ravi Kumar, M. N. V. A review of chitin and chitosan applications. *React. Funct. Polym.* **2000**, *46*, 1−27.
(61) Kümmerer, K.; Dionysiou, D. D.; Olsson, O.; Fatta-Kassinos, D. A path to clean water. *Science* **2018**, *361*, 222−224.
(62) Varga, R.; Somogyvári, I.; Eke, Z.; Torkos, K. Determination of antihypertensive and anti-ulcer agents from surface water with solid-phase extraction−liquid chromatography−electrospray ionization tandem mass spectrometry. *Chemosphere* **2011**, *83*, 1447−1454.
(63) Daneshvar, A.; Svanfelt, J.; Kronberg, L.; Prévost, M.; Weyhenmeyer, G. A. Seasonal variations in the occurrence and fate of basic and neutral pharmaceuticals in a Swedish river-lake system. *Chemosphere* **2010**, *80*, 301−309.
(64) Fraysse, B.; Garric, J. Prediction and experimental validation of acute toxicity of β-blockers in *Ceriodaphnia dubia*. *Environ. Toxicol.* **2005**, *24*, 2470−2476.
(65) Blake, S. C.; Daniel, B. S.; Daniel, B. S. Cutaneous lupus erythematosus: A review of the literature. *Int. J. Women. Dermatol.* **2019**, *5*, 320−329.
(66) Fan, M.; Hu, Q.; Shen, K. Preparation and structure of chitosan soluble in wide pH range. *Carbohydr. Polym.* **2009**, *78*, 66−71.
(67) Nie, J.; Wang, Z.; Hu, Q. Difference between chitosan hydrogels via alkaline and acidic solvent systems. *Sci. Rep.* **2016**, *6*, 36053.
(68) Li, P.; Zhao, J.; Chen, Y.; Cheng, B.; Yu, Z.; Zhao, Y.; Yan, X.; Tong, Z.; Jin, S. Preparation and characterization of chitosan physical hydrogels with enhanced mechanical and antibacterial properties. *Carbohydr. Polym.* **2017**, *157*, 1383−1392.
(69) Brandiele, R.; Durante, C.; Grądzka, E.; Rizzi, G. A.; Zheng, J.; Badocco, D.; Centomo, P.; Pastore, P.; Granozzi, G.; Gennaro, A. One step forward to a scalable synthesis of platinum−yttrium alloy nanoparticles on mesoporous carbon for the oxygen reduction reaction. *J. Mater. Chem. A* **2016**, *4*, 12232−12240.
(70) Thiam, A.; Salazar, R.; Brillas, E.; Sirés, I. Electrochemical advanced oxidation of carbofuran in aqueous sulfate and/or chloride media using a flow cell with a RuO_2-based anode and an air diffusion cathode at pre-pilot scale. *Chem. Eng. J.* **2018**, *335*, 133−144.
(71) Thommes, M.; Kaneko, K.; Neimark, A. V.; Olivier, J. P.; Rodriguez-Reinoso, F.; Rouquerol, J.; Sing, K. S. W. Physisorption of gases, with special reference to the evaluation of surface area and pore size distribution (IUPAC Technical Report). *Pure Appl. Chem.* **2015**, *87*, 1051−1069.
(72) Trevisanello, E.; De Bon, F.; Daniel, G.; Lorandi, F.; Durante, C.; Isse, A. A.; Gennaro, A. Electrochemically mediated atom transfer radical polymerization of acrylonitrile and poly(acrylonitrile-b-butyl acrylate) copolymer as a precursor for N-doped mesoporous carbons. *Electrochim. Acta* **2018**, *285*, 344−354.
(73) Brandiele, R.; Zerbetto, M.; Dalconi, M. C.; Rizzi, G. A.; Isse, A. A.; Durante, C.; Gennaro, A. Mesoporous carbon with different density of thiophenic-like functional groups and their effect on oxygen reduction. *ChemSusChem* **2019**, *12*, 4229−4239.
(74) Brandiele, R.; Poli, F.; Picelli, L.; Pilot, R.; Rizzi, G. A.; Soavi, F.; Durante, C. Nitrogen-doped mesoporous carbon electrodes prepared from templating propylamine-functionalized silica. *ChemElectroChem* **2020**, *7*, 1914−1921.
(75) Bezerra, C. W. B.; Zhang, L.; Lee, K.; Liu, H.; Marques, A. L. B.; Marques, E. P.; Wang, H.; Zhang, J. A review of Fe-N/C and Co-N/C catalysts for the oxygen reduction reaction. *Electrochim. Acta* **2008**, *53*, 4937−4951.
(76) Ferrari, A. C.; Robertson, J. Interpretation of Raman spectra of disordered and amorphous carbon. *Phys. Rev. B* **2000**, *61*, 14095−14107.
(77) Perazzolo, V.; Grądzka, E.; Durante, C.; Pilot, R.; Vicentini, N.; Rizzi, G. A.; Granozzi, G.; Gennaro, A. Chemical and electrochemical stability of nitrogen and sulphur doped mesoporous carbons. *Electrochim. Acta* **2016**, *197*, 251−262.
(78) Salmerón, I.; Plakas, K. V.; Sirés, I.; Oller, I.; Maldonado, M. I.; Karabelas, A. J.; Malato, S. Optimization of electrocatalytic H_2O_2 production at pilot plant scale for solar-assisted water treatment. *Appl. Catal., B* **2019**, *242*, 327−336.
(79) Steter, J. R.; Brillas, E.; Sirés, I. On the selection of the anode material for the electrochemical removal of methylparaben from different aqueous media. *Electrochim. Acta* **2016**, *222*, 1464−1474.
(80) Isarain-Chávez, E.; Arias, C.; Cabot, P. L.; Centellas, F.; Rodríguez, R. M.; Garrido, J. A.; Brillas, E. Mineralization of the drug β-blocker atenolol by electro-Fenton and photoelectro-Fenton using an air-diffusion cathode for H_2O_2 electrogeneration combined with a carbon-felt cathode for Fe^{2+} regeneration. *Appl. Catal., B* **2010**, *96*, 361−369.
(81) Píšťková, V.; Tasbihi, M.; Vávrová, M.; Štangar, U. L. Photocatalytic degradation of β-blockers by using immobilized

https://dx.doi.org/10.1021/acssuschemeng.0c04294
ACS Sustainable Chem. Eng. 2020, 8, 14425−14440

titania/silica on glass slides. *J. Photochem. Photobiol., A* **2015**, *305*, 19−28.
(82) Xu, A.; Brillas, E.; Han, W.; Wang, L.; Sirés, I. On the positive effect of UVC light during the removal of benzothiazoles by photoelectro-Fenton with UVA light. *Appl. Catal., B* **2019**, *259*, 118127.
(83) Nsubuga, H.; Basheer, C.; Jalilov, A.; Haider, M. B.; Al-Saadi, A. A. Droplet flow-assisted heterogeneous electro-Fenton reactor for degradation of beta-blockers: response surface optimization, and mechanism elucidation. *Environ. Sci. Pollut. Res.* **2019**, *26*, 14313−14327.

https://dx.doi.org/10.1021/acssuschemeng.0c04294
ACS Sustainable Chem. Eng. 2020, 8, 14425−14440